THE GEOLOGICAL SOCIETY OF AMERICA®

Linking an Early Triassic delta to antecedent topography: Source-to-sink study of the southwestern Barents Sea margin

Christian Haug Eide[1,†], Tore G. Klausen[1], Denis Katkov[2], Anna A. Suslova[2], and William Helland-Hansen[1]
[1]*Department of Earth Science, University of Bergen, Box 7803, 5020 Bergen, Norway*
[2]*Petroleum Department, Moscow State University, Moscow, 119991, Russia*

ABSTRACT

Present-day catchments adjacent to sedimentary basins may preserve geomorphic elements that have been active through long intervals of time. Relicts of ancient catchments in present-day landscapes may be investigated using mass-balance models and can give important information about upland landscape evolution and reservoir distribution in adjacent basins. However, such methods are in their infancy and are often difficult to apply in deep-time settings due to later landscape modification.

The southern Barents Sea margin of N Norway and NW Russia is ideal for investigating source-to-sink models, because it has been subject to minor tectonic activity since the Carboniferous, and large parts have eluded significant Quaternary glacial erosion. A zone close to the present-day coast has likely acted as the boundary between basin and catchments since the Carboniferous. Around the Permian-Triassic transition, a large delta system started to prograde from the same area as the present-day largest river in the area, the Tana River, which has long been interpreted to show features indicating that it was developed prior to present-day topography. We performed a source-to-sink study of this ancient system in order to investigate potential linkages between present-day geomorphology and ancient deposits.

We investigated the sediment load of the ancient delta using well, core, two-dimensional and three-dimensional seismic data, and digital elevation models to investigate the geomorphology of the onshore catchment and surrounding areas. Our results imply that the present-day Tana catchment was formed close to the Permian-Triassic transition, and that the Triassic delta system has much better reservoir properties compared to the rest of Triassic basin infill. This implies that landscapes may indeed preserve catchment geometries for extended periods of time, and it demonstrates that source-to-sink techniques can be instrumental in predicting the extent and quality of subsurface reservoirs.

INTRODUCTION

An understanding of the mass balances from catchments to ultimate sediment sinks is important because they illuminate the links between long-term mass fluxes and filling of sedimentary basins, and the patterns of erosion and denudation that record Earth history (Bhattacharya et al., 2016; Helland-Hansen et al., 2016). It is also important in order to predict sedimentary environments and their link to catchments in areas with limited data (e.g., Sømme et al., 2009a), since it increases predictability in reservoir and hydrocarbon exploration (Martinsen et al., 2010). Investigating sediment mass balances for source-to-sink systems in deep time (≤10^8 yr) is challenging because factors such as tectonic regime and climate are poorly constrained, catchments are largely eroded, and resolution of dating methods is uncertain (e.g., Romans et al., 2016; Helland-Hansen et al., 2016). However, in the Early Triassic of the Barents Sea, several of these hampering issues are alleviated: Biostratigraphic dating has a relatively high resolution (~1 m.y.) due to rapid evolutionary diversification after the Permian-Triassic extinction event (e.g., Chen and Benton, 2012); the climate during this period has been the subject of several studies, as it was a time of major climatic shifts (Péron et al., 2005; Sellwood and Valdes, 2006; Svensen et al., 2009; Hochuli and Vigran, 2010; Sun et al., 2012); and minor tectonic change has occurred in this area since the Carboniferous (Bugge et al., 1995; Riis, 1996; Gudlaugsson et al., 1998; Hall, 2015). The present-day Fennoscandian Barents Sea coast (Fig. 1) is likely a close approximation to the long-term boundary between the successive sedimentary basins located in the Barents Sea and the eroding uplands of the Fennoscandian Shield (e.g., Worsley, 2008; Hall, 2015). The area has also largely escaped extensive modification by Quaternary glaciations (Riis, 1996; Ebert et al., 2015; Hall et al., 2015) and is therefore an ideal location in which to test and develop models for linking ancient sedimentary systems to catchments.

Because distinct sediment source areas may produce sand types with dramatically different reservoir properties, it may be critical in reservoir exploration settings to understand the amount of sediment produced from different catchments, because this will help to predict the distribution and extent of suitable sandstones. The Norwegian Barents Sea is an area of ongoing petroleum exploration, but the Triassic strata generally show poor reservoir properties. This is mainly because the majority of the sandstones were sourced from the young and active Uralian orogen through an enormous fluvial system, stretching over 1.2 × 10^3 km from the Urals in the SE to at least Svalbard in the NW (Figs. 1, 2B, and 3; Bergan and Knarud, 1993; Mørk, 1999; Glørstad-Clark et al., 2010; Klausen et al., 2015). This led to the deposition of mineralogically immature and mudstone-rich sediments, and, due to long transport and decreasing gradients, extraction of coarse grains before the fluvial system reached the present Norwegian sector.

Several authors have briefly described a sedimentary system with more favorable reservoir properties prograding from the Fennoscandian Shield to the south into the Finnmark Platform in the Barents Sea Basin during the earliest Induan (earliest Triassic; Fig. 2; Hadler-Jacobsen

†christian.eide@uib.no

GSA Bulletin; January/February 2018; v. 130; no. 1/2; p. 263–283; https://doi.org/10.1130/B31639.1; 13 figures; 1 table; Data Repository item 2017267; published online 15 August 2017.

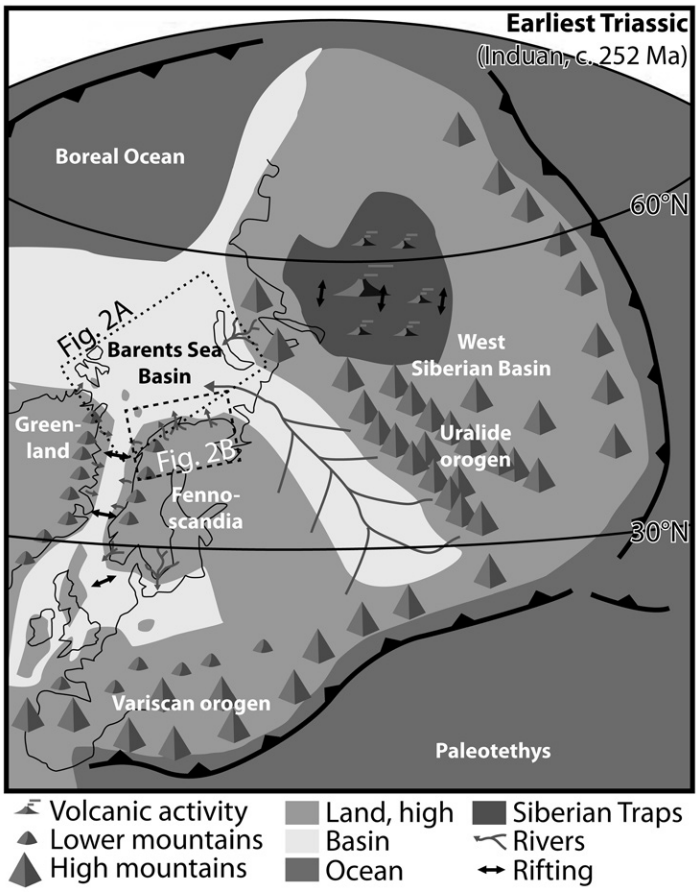

Figure 1. Paleogeographic map showing regional setting of the study area in the Early Induan (Early Triassic). Based on a variety of sources, including Cocks and Torsvik (2006), McKie and Williams (2009), Reichow et al. (2009), and Miller et al. (2013).

et al., 2005; Glørstad-Clark et al., 2010; Henriksen et al., 2011a). This system appears to have been point sourced, and it is fully constrained by high-quality two-dimensional (2-D) seismic data. The system has been sampled by three available shallow cores (Mangerud, 1994; Bugge et al., 1995) and industry well logs, and it is therefore well suited for a source-to-sink analysis. Furthermore, the Tana and Alta River systems directly onshore in northernmost Norway have long been interpreted to show numerous antecedent features (NE-flowing tributary channels deeply incised into the generally SSE-dipping topographic trend of N Fennoscandia, and a highly asymmetric tributary pattern; Fig. 2A; e.g., Gjessing, 1978), and we make the case that at least the Tana River drainage network had already developed around the Permian-Triassic transition.

The objectives of this paper are fivefold: (1) to describe the southerly Induan system in the Barents Sea based on available 2-D and three-dimensional (3-D) seismic, core, and well data, (2) to investigate mass-balance and source-to-sink-relationships of this system to constrain catchment properties, (3) to investigate possible links to relict onshore catchment geometries, (4) to discuss the impact of this analysis on reservoir prediction in the Barents Sea, and (5) to demonstrate the applicability of source-to-sink models to reservoir exploration in general.

GEOLOGICAL BACKGROUND

The northern Fennoscandian margin has acted as a boundary between the mainly emergent Fennoscandian Shield and the Barents Sea Basin (Fig. 1) since the late Proterozoic, and it represents a long-lasting hinge line separating areas of net uplift on the shield from areas of net subsidence in the basin (Hall, 2015). The Troms-Finnmark fault zone is the main boundary between the basin and the mainland on the western Finnmark Platform, and the Austhavet fault zone is the main boundary on the eastern Finnmark Platform (Fig. 2A; Roberts and Lippard, 2005). From the Ordovician through the Devonian, the Fennoscandian Shield was buried by foreland basin sediments related to the Caledonian orogeny (490–390 Ma), which were later eroded (Larson et al., 1999, 2006; Kohn et al., 2009). Several NE-SW–oriented rift zones were formed in the Barents Sea Basin during the middle Carboniferous (Gudlaugsson et al., 1998). This affected sediment transport networks, e.g., by funneling a major delta system out a half-graben along the present-day Porsangerfjorden (Fig. 2A; Bugge et al., 1995). During the late Carboniferous, the Barents Sea Basin entered an intracratonic sag phase and was dominated by regional subsidence (Gudlaugsson et al., 1998). From the late Carboniferous to the latest Permian, the Barents Sea Basin was the site of a regional carbonate platform, with minor clastic input from nearby landmasses (Bugge et al., 1995; Samuelsberg et al., 2003; Colpaert et al., 2007). Gradual northward drift of the continent during the Permian led to gradual cooling and a change from tropical reefs to cool-water spiculitic carbonates in the Kungurian ("middle" Permian; e.g., Worsley, 2008).

Major changes occurred around the Permian-Triassic transition, both in terms of climate and regional tectonic setting. A marked lithological change occurs across the western part of the basin close to this boundary, from the cool-water carbonates and spiculitic shales of the Tempelfjorden Group to the shale-dominated Sassendalen Group (Fig. 3; e.g., Mørk et al., 1982; Wignall et al., 1998; Vigran et al., 2014). A major rise in global average temperature of ~15 °C occurred at this time, leading to the greatest mass extinction recorded (Sun et al., 2012). This event has been linked to major eruptions and gas release in the Siberian Traps large igneous province (Svensen et al., 2009; Reichow et al., 2009; Burgess and Bowring, 2015).

This time also coincided with the start of progradation of a major sedimentary system (prodelta–delta–delta plain) of the Havert Formation out of the Uralian foreland basin and Kara Sea into the Barents Sea Basin (Fig. 3C; Puchkov, 2009; Glørstad-Clark et al., 2010; Norina et al., 2014). At the same time, around the Permian-Triassic transition (Vigran et al., 2014), smaller sedimentary systems started to prograde from the Fennoscandian Shield into the Barents Sea Basin (Glørstad-Clark et al., 2010; Henriksen et al., 2011a; Hall, 2015), and from Greenland into the Barents Sea Basin in Svalbard (Fig. 3C; Mørk et al., 1982; Wignall et al., 1998). This was coincident with rifting of the western Norwegian–eastern Greenland margins in the latest Permian and earliest Triassic

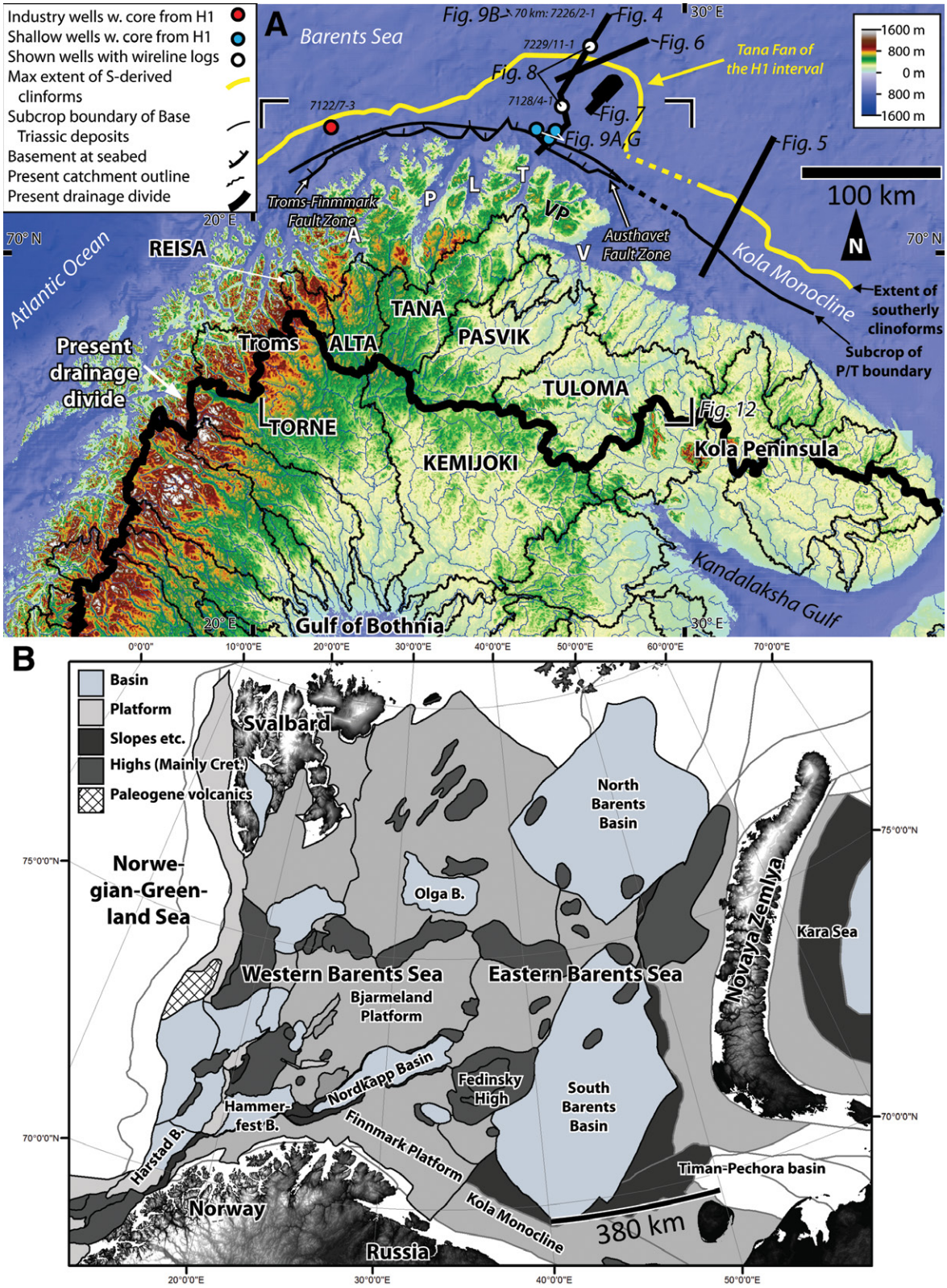

Figure 2. (A) Topography of the study area, with catchments larger than 5×10^3 km^2, and location of presented figures and data. Capitalized names written in full are names of catchments. A—Altafjord; P—Porsangerfjorden; L—Laksefjord; T—Tanafjord; V—Varangerfjord; VP—Varanger Peninsula; P/T—Permian-Triassic. (B) Important structural elements in the Barents Sea and surrounding areas. Note that the entire Barents Sea subsided during the Triassic, and that few of these structural elements had a significant influence on the Triassic basin infill. B—Basin.

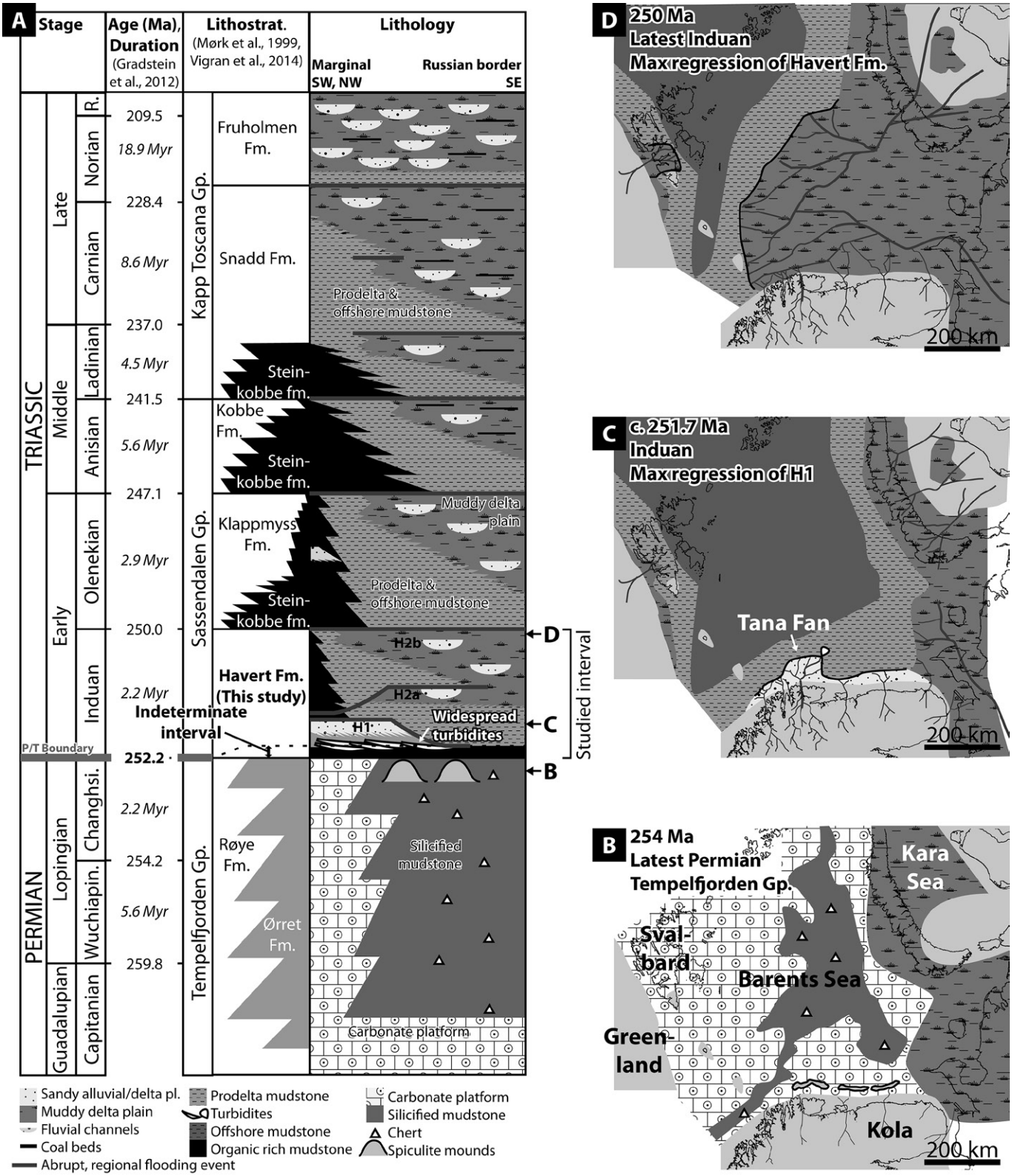

Figure 3. (A) Lithostratigraphy of the Barents Sea, based on Mørk et al. (1999) and Vigran et al. (2014). (B) Paleogeography during deposition of the Tempelfjorden Group in the latest Permian. (C) Early Induan paleogeography during maximum regression of the H1 interval of the Havert Formation. Note the large fan-shaped protrusion in the paleocoastline, termed the Tana fan. (D) Late Induan paleogeography during maximum regression of Havert Formation. B–D are based on Glørstad-Clark et al. (2010); Henriksen et al. (2011a); Norina et al. (2014); and work presented herein (H1). P/T—Permian-Triassic.

(Ziegler, 1992; Müller et al., 2005; Faleide et al., 2008; Stoker et al., 2016), and it may possibly be explained by dynamic rift-shoulder uplift (cf. Wernicke, 1985; ten Brink and Stern, 1992; Daradich et al., 2003), which may have led to increased topography, and thus increased erosion rates and sediment supply, and therefore progradation of sedimentary systems.

Overall, the southern Barents Sea Basin subsided through the remainder of the Triassic and was infilled by several kilometers of sediment of the Klappmyss, Kobbe, and Snadd Formations, mainly derived from the Uralian orogen and Kara Sea (Fig. 3; Glørstad-Clark et al., 2010; Henriksen et al., 2011a; Pózer Bue and Andresen, 2014; Klausen et al., 2015). After the arrival of the easterly derived Uralian system on the Finnmark Platform, the southerly system cannot be identified in seismic data. In the Early Jurassic, the majority of sediment deposited in the Barents Sea was derived from Fennoscandia, but sediment volumes, and hence erosion rates, were low (Ryseth, 2014). This led to improved reservoir properties in the Lower Jurassic interval, due to widespread sediment recycling and reduced input of immature sediment from the Uralian orogeny (Ryseth, 2014). During the Late Jurassic and Early Cretaceous high sea level, the southern source area was then buried by sediment due to flooding (Riis, 1996; Hendriks and Andriessen, 2002), along with the majority of Fennoscandia (Fossen et al., 1997; Bøe et al., 2010; Lidmar-Bergström et al., 2013). This may have led to preservation of the Triassic–Early Jurassic catchments beneath a sedimentary cover.

Rifting along the western Norwegian margin continued intermittently from the Triassic until final breakup between Norway and Greenland during the Eocene (Talwani and Eldholm, 1977; Faleide et al., 2008). The final breakup led to development and intensification of high topography along western Norway (Redfield and Osmundsen, 2013), but a similar topography had likely existed prior to breakup due to rift shoulder uplift through multiple rifting events (e.g., Lidmar-Bergström et al., 2013; Sømme et al., 2009b). The study area, located on the Finnmark Platform (Fig. 2A), remained largely unaffected by significant deformation during these rift phases (Gudlaugsson et al., 1998).

During the Cenozoic, the southern Barents Sea Basin and Fennoscandia were mainly in a state of uplift and erosion (Henriksen et al., 2011b; Laberg et al., 2012; Baig et al., 2016). The total erosion along the southern Barents Sea is estimated at ~1200 m, and approximately half of this is estimated to be due glacial erosion during the last 2.7 m.y. (Laberg et al., 2012; Baig et al., 2016). The erosion onshore in northern Fennoscandia is uncertain. Fission-track studies from NE Norway have yielded old cooling ages, indicating minor exhumation since the Permian–mid-Triassic (Hendriks and Andriessen, 2002; Hendriks et al., 2007). Several lines of geomorphological evidence indicate near-negligible glacial erosion of low-relief bedrock surfaces in northern Finland and Sweden (Ebert et al., 2015; Hall et al., 2015). Quaternary glaciations led to development of extensive fjords in the study area through deepening of preexisting valleys, particularly in the outer reaches (Fig. 2A; Lidmar-Bergström, 2013; Winsborrow et al., 2010; cf. Nesje and Whillans, 1994). However, several coastal midaltitude (200–600 m above sea level) plateaus on the NE Norwegian coast, particularly the Varanger Peninsula (Fig. 2A), are mantled by extensive block fields and show clear evidence of having survived despite being covered by ice during at least the most recent glaciation (Fjellanger et al., 2006; Fjellanger and Sørbel, 2007). This indicates that the costal plateaus are potentially very old landscape features. These plateaus have been interpreted by Riis (1996) to represent remnants of an early Mesozoic peneplain (cf. Lidmar-Bergström et al., 2013).

DATA SET

Several complementary data sets were utilized for this study of the Finnmark Platform, the Kola monocline, and surrounding land areas in northern Fennoscandia (Fig. 2). The subsurface in Norway was studied in a set of several intersecting 2-D seismic lines with a typical spacing of 5–10 km, one 3-D seismic cube with an extent of 25 × 70 km, industry wireline log data, and exploration and shallow research cores available from the Norwegian Petroleum Directorate. The shallow research cores (e.g., Bugge et al., 1995) are distinguished with a "U" in their well number, as in the case of 7128/12-U-01 (cf. Fig. 4). The subsurface in the Russian sector was investigated using a set of 2-D seismic lines spaced 45–90 km apart. The geomorphological part of the study (Fig. 2) was performed on several high-resolution topographic and bathymetric data sets available from the Norwegian Mapping Authority and the National Land Survey of Finland, and regional topographical and bathymetrical data (Jakobsson et al., 2012).

Relevant stratigraphic horizons were tied to published, biostratigraphically dated boundaries in wells, available as well tops from the Norwegian Petroleum Directorate. Depth and mass conversion was performed using velocity and density data from intersecting wireline logs and published velocity profiles from shallow cores (Bugge et al., 1995).

OBSERVATIONS FROM INDUAN PROGRADING SYSTEMS

The Induan (earliest Triassic) succession in the southwestern Barents Sea is represented by the Havert Formation of the Sassendalen Group (Fig. 3A; Mørk et al., 1999), which is time-equivalent to the Vardebukta Formation on western Svalbard (e.g., Mørk et al., 1982, 1999; Wignall et al., 1998; Vigran et al., 2014). The Havert Formation was subdivided into two subsequences by Glørstad-Clark et al. (2010), which are here termed H1 and H2 (Fig. 3). The H2 interval may be further subdivided into H2a and H2b, but the implications of this are beyond the scope of this paper. The H1 interval prograded from the south (Fig. 3C), and the H2 interval prograded from the east (Fig. 3D). The main focus of this paper is the H1 interval, but it is also compared to the younger H2 interval. The section starts with an overall description of the setting and morphology from 2-D seismic data, followed by descriptions of plan-view geometries from 3-D seismic data, petrophysical properties, and sedimentary environments from well and core data, and mineralogical and clast composition data compiled from previous work. The section ends with a discussion of paleocurrent data, thickness trends, and estimation of mass balances.

Regional Setting

The regional composite seismic line presented in Figure 4 describes the overall depositional setting on the eastern Finnmark Platform. The depth to basement shallows toward the mainland, and the sedimentary strata are uplifted toward the mainland and finally truncated toward the base Quaternary unconformity. The sedimentary strata all show gradual thinning toward the mainland, indicating that accommodation has decreased toward the basin margin throughout time. An abrupt rise in depth to basement occurs over the Austhavet fault zone. The studied H1 interval is visible as a prominent, northward-prograding clinoform package above the Permian Tempelfjorden Group.

Overall Shoreline Morphology

The H1 interval is present from Troms in the west to at least the central Kola Peninsula in the east (Figs. 2A and 5). The Triassic succession rises in depth toward the mainland and subcrops below the Quaternary cover 30–60 km from the

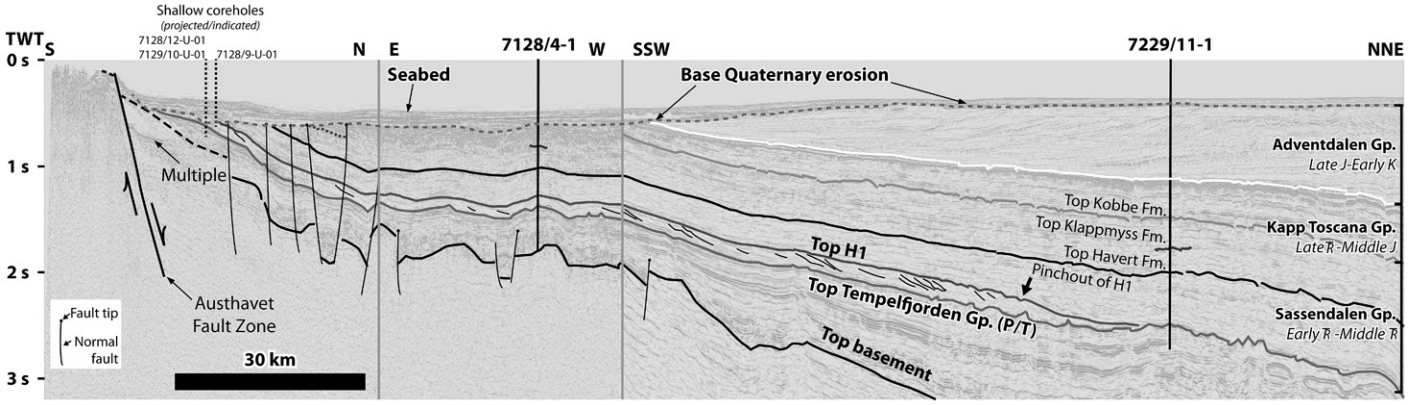

Figure 4. Interpreted composite two-dimensional seismic line from the Norwegian mainland to the Nordkapp Basin showing regional development of sedimentary systems on the Finnmark Platform. Note the thinning of sedimentary units toward the mainland (southward), erosional truncation of sediment packages toward the mainland, and the gradual basinward (northward) thickening and abrupt pinchout of the clinoformal H1 interval. For location, see Figure 2A. See supplementary material S01 for an uninterpreted version.[1] TWT—two-way traveltime; P/T—Permian-Triassic; TR—Triassic; J—Jurassic; K—Cretaceous.

present-day coastline (Figs. 2, 4, and 5). The most seaward clinoform break prograded to ~30 km north of the subcrop line along the entire margin, apart from around Tanafjord, where a 175-km-wide, lobate protrusion prograded to ~100 km from the subcrop line (Fig. 2A). We term this protrusion the Tana fan of the H1 interval (Fig. 3C). The system is interpreted to represent a large prograding delta system that built out from Fennoscandia during the Induan. The Tana fan around Tanafjord is interpreted to represent a major deltaic edifice along this shoreline. The Fennoscandian-derived H1 interval is covered (downlapped) by prograding clinoforms of the H2 system, which prograded from the east (Fig. 6).

Planform Geometries from 3-D Seismic Data

The available 3-D seismic data clearly show the prograding clinoforms of the H1 interval overlying the Tempelfjorden Group (Fig. 7A). The clinoforms generally exhibit a tangential oblique morphology, and they prograded toward the NNE (Figs. 7C–7D). Toesets in the H1 interval commonly show localized high-amplitude reflectors, and in amplitude maps, these exhibit a branching distributary pattern interpreted as a sand-filled turbidite fan (Fig. 7B; see also Hadler-Jacobsen et al., 2005). Similar localized high-amplitude anomalies are also located on 2-D seismic lines elsewhere within the Tana fan, indicating that turbidite fans are common within the bottomset of the deltaic Tana fan of the H1 system all over the Finnmark Platform. Topsets in the H1 interval show diffuse, laterally extensive, high-amplitude reflections without any clearly indicative seismic geomorphologies. These may indicate a sandy braidplain, an interpretation mainly based on sedimentological data presented later herein.

Above the boundary to the overlying H2 interval, a marked shift in sediment transport directions and fluvial style occurs. Clinoform progradation directions are toward the NW across the basin in this interval. In the upper parts of the H2 interval, discrete NW-directed, 0.2–4-km-wide, high-amplitude, meandering ribbons occur, some showing scroll-bar patterns (Fig. 7E). These are interpreted to represent fluvial channels on a delta plain, sourced from the easterly Uralian orogen, and they are similar to fluvial channels described for the later Triassic formations in the basin (cf. Klausen et al., 2014).

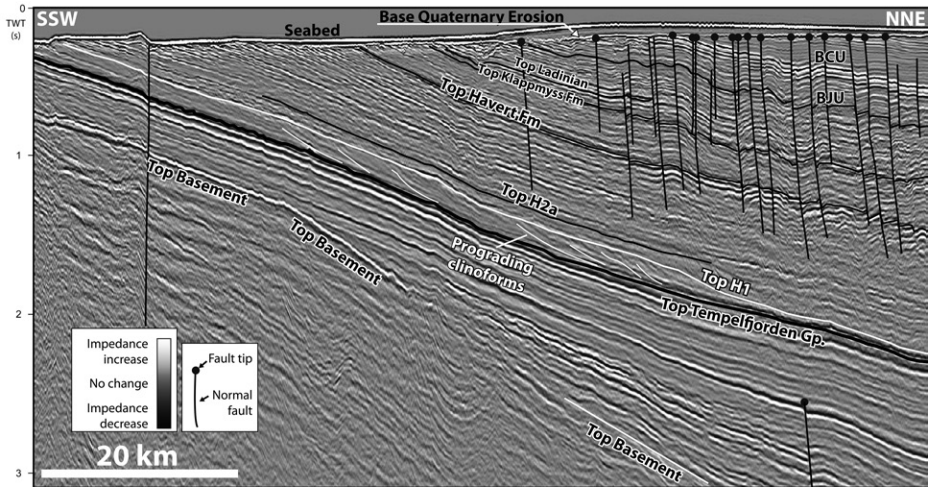

Figure 5. Interpreted two-dimensional seismic line from the Kola monocline, showing the same, northward-prograding system just above the top of the Permian carbonate platform succession in the Russian sector. For location, see Figure 2. For uninterpreted version, see supplementary material S02 (see text footnote 1). BJU—base Jurassic unconformity; BCU—base Cretaceous unconformity. TWT—two-way traveltime.

Well and Core Data

Three exploration wells that penetrate the Havert Formation on the Finnmark Platform

[1]GSA Data Repository item 2017267, uninterpreted versions of Figures 4, 5, and 6, is available at http://www.geosociety.org/datarepository/2017 or by request to editing@geosociety.org.

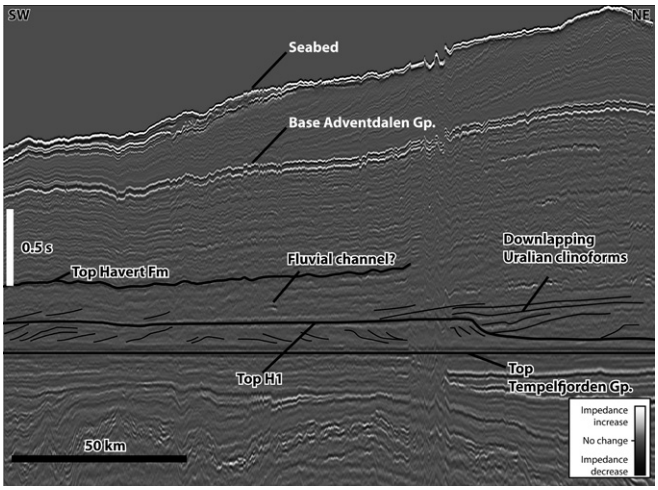

Figure 6. Interpreted two-dimensional seismic line from the Finnmark Platform showing downlap of the easterly H2 interval on the northward-prograding H1 interval. Seismic line is flattened on the top of the Tempelfjorden Group, which approximates the Permian-Triassic boundary. For location, see Figure 2. For uninterpreted version, see supplementary material S03 (see text footnote 1).

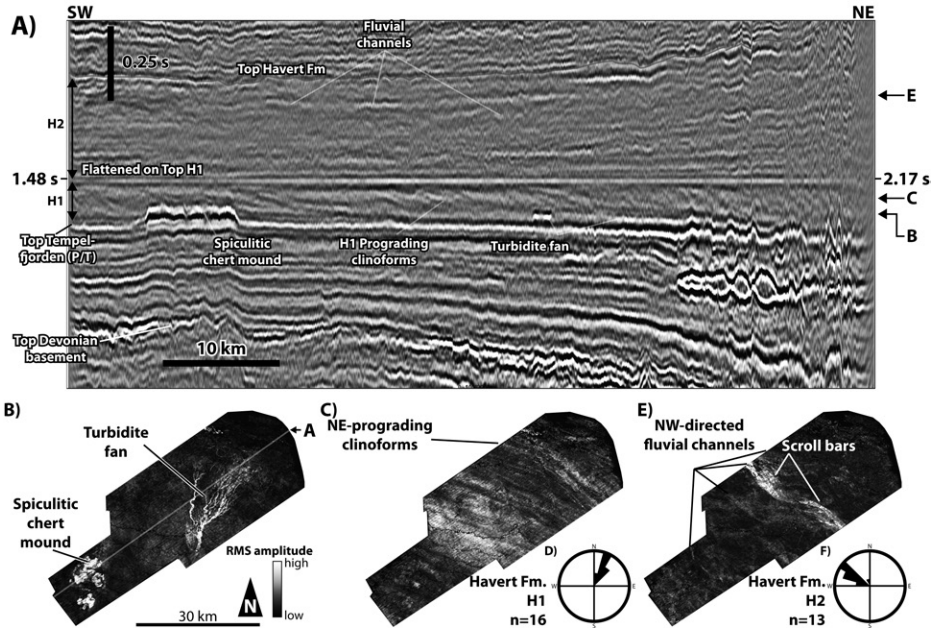

Figure 7. Three-dimensional (3-D) seismic data from the Tana fan. (A) Inline 1949 from the 3-D seismic survey, flattened on top of the H1 interval (for location, see Fig. 2). Note the prominent, steeply dipping clinoforms, the gradual thickening of the clinoform package to the NW, and the amplitude anomalies interpreted as a turbidite fan in the bottomset. P/T—Permian-Triassic transition. (B) Amplitude map from the bottomset of the Tana fan of the H1 interval showing a high-amplitude distributary pattern interpreted as turbidite channels and lobes. (C) Amplitude map intersecting the clinoforms of the H1 interval. (D) Paleocurrents from clinoforms, turbidite fan, and fluvial channels imaged in amplitude maps in the Tana fan of the H1 interval. (E) Amplitude map from the H2 interval of the Havert Formation (above the H1 interval), showing abundant NW-directed fluvial channels. (F) Paleocurrents measured from fluvial channels imaged in amplitude maps in the H2 interval of the Havert Formation. Note the change in paleocurrent directions compared to the underlying Tana fan of the H1 interval in D. RMS—Root Mean Square.

are currently available for study (Figs. 2 and 8; wells 7128/11-1, 7128/6-1, and 7128/4-1). The wireline log data show considerable difference between the topsets of the H1 interval (dotted in Fig. 8) and of the rest of the Havert Formation (Fig. 8). Most importantly, the gamma-ray log shows consistently low readings in the topsets of the H1 interval, indicating sand-rich topsets (Fig. 8). The H2 interval of the Havert Formation shows higher gamma-ray readings interrupted by spikes and sharp falls with gradual upward-increasing readings, interpreted to represent an overall mud-rich delta plain with occasional upward-fining fluvial channels (Fig. 8). This environment is similar to that found in the remainder of the Uralian-derived Triassic succession in the majority of the Barents Sea (cf. Klausen et al., 2015).

All available core data of the Havert Formation were investigated for this study, and details about sedimentological interpretations are substantiated in Table 1. Four cored sections exist for the H1 interval, with a total length of 83.5 m; three of these were acquired by drilling of shallow stratigraphic core holes (Bugge et al., 1995). Nine cored sections are available for the H2 interval of the Havert Formation, with a total length of 128 m.

The shallow stratigraphic cores are located at the subcrop line near Tanafjord and sample the Tana fan of the H1 interval (Figs. 2, 4, and 9). Two of these were drilled with the objective of sampling the Permian-Triassic transition and immediate surroundings (Fig. 9G; Mangerud, 1994), and thus they sample the condensed Permian spiculitic mudstones and limestones of the Røye Formation of the Tempelfjorden Group and the toesets of the H1 interval (Fig. 9G). Between the Changshingian (latest Permian) of the Tempelfjorden Group and the Induan (earliest Triassic), an ~12 m interval of indeterminate age exists (Fig. 9G; Vigran et al., 2014). However, the lowermost 24 m section of the Havert Formation, including the 12 m of indeterminate age, consists of mudstones interbedded with abundant 1–60-cm-thick turbidites (Fig. 9G; Table 1). These are interpreted as turbidites fed from a prograding delta (Table 1), in accordance with what is seen in the 3-D seismic cube (Fig. 7B). The overlying parts of the core are more mudstone-rich, with occasional thin turbidites and a general upward increase in the amount of wave-rippled sandstone beds (Fig. 9G). Thus, these two cores are interpreted to show the transition from basal turbidite fans to lower prodelta slope clinoforms, which show only minor wave influence, to shallower, upper prodelta slope clinoforms where wave processes are more influential (Table 1).

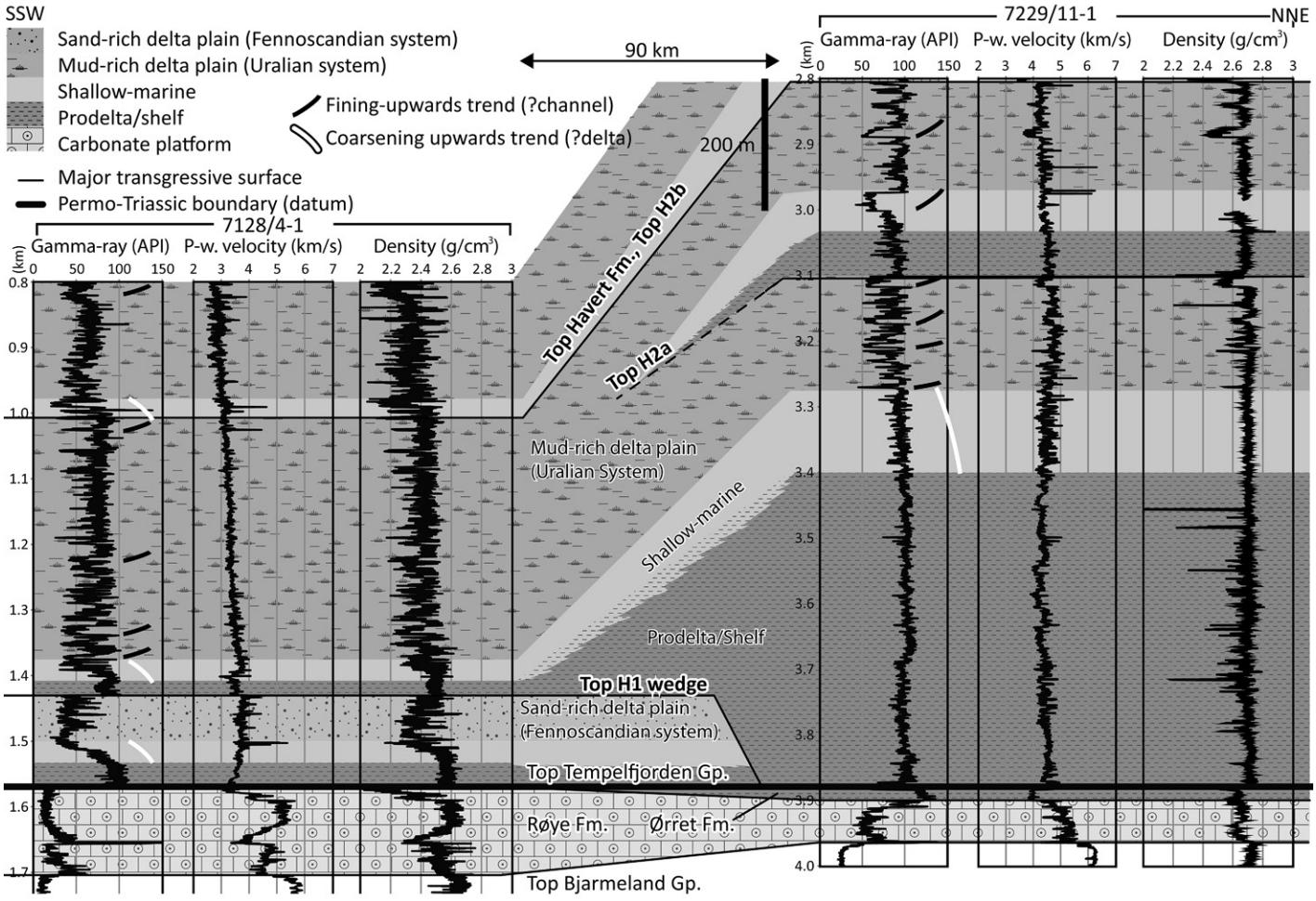

Figure 8. Interpretation and correlation of industry wireline logs penetrating the Havert Formation. See Figures 2, 4, and 11 for location. Note the low gamma-ray values in the H1 topset interval (dotted) compared to the high to variable gamma-ray values in the remainder of the Havert Formation (striped), indicating that the H1 interval is much more sandstone-rich than the overlying system. P-w—P-wave; API—natural downhole radioactivity, which generally scales with shale content.

Shallow core 7128-9-U-01 (Figs. 2A, 4, and 9A) was drilled with the goal to core the entire H1 interval, but it was terminated due to drilling problems, likely due to the drill bit sticking on large extraformational clasts. Only parts of the H1 topsets are therefore recorded. The core shows a wide variety of depositional facies (Fig. 9A; Table 1). Facies FA7 is composed of uncemented, well-sorted, fine-grained sand with cross-beds, interpreted as shoreface deposits (Table 1). Facies FA8 is made up of sharp-based, polymict conglomerates with abundant well-rounded extraformational sedimentary and crystalline clasts and sandstone matrix, interpreted as proximal fluvial channels (Fig. 9C; Table 1). Facies FA9 consists of 1–20 cm sandstone beds with undifferentiated ripples, sparse *Arenicolites* and *Planolites* burrows, and extraformational sedimentary clasts, interbedded with wavy-bedded mudstones, interpreted as tidal flats. Facies FA10 is composed of intensely red homogeneous siltstone beds with abundant white rhizocretions (root structures encased in concretionary material), capped by a synsedimentary brecciated interval interpreted as a paleosol. Facies FA11 is well-sorted, greenish, fine-grained sandstone with abundant rhizocretions (Fig. 9D), interpreted as a pedogenized version of facies FA9. This is entire system is interpreted as deposits of a sandy braidplain proximal to a delta influenced by mainly river currents, but occasionally reworked by tides and waves. The deep-red soil color and abundant rhizocretions indicate a semiarid climate (cf. Mack and James, 1994; Nystuen et al., 2014).

Only one available core exists from the H1 interval outside Tana fan. This core is from the well 7122/7-3 in the Goliat field, 220 km to the WSW of the shallow cores (Fig. 2A). The core is 2 m long, and it consists of pebbly medium- to very coarse-grained sandstone. This facies is similar to that observed in FA8 (interpreted as fluvial channels) in the H1 interval (Table 1; cf. Fig. 9A). Such grain sizes are not seen elsewhere in the Uralian-derived Triassic deposits of the Barents Sea, and they indicate that the entire H1 interval was sourced from the Fennoscandian Shield.

A log through a cored section of the easterly derived H2 interval in well 7226/2-1 (for location, see Fig. 2) is presented here for comparison with the southerly derived H1 interval (cf. Figs. 9A and 9B). The presented section mainly contains the following facies (Table 1): Facies FA12 is laminated mudstone with abundant sandy pinstripes, 1–10-cm-thick, sharp-based beds of normal-graded very fine-grained sandstone (thin turbidites), and 1–10-cm-thick rippled sandstone beds, interpreted as delta-front deposits. Facies FA13 is composed of very

TABLE 1. SUMMARY DESCRIPTIONS OF FACIES ASSOCIATIONS

Facies association	Bedding and lithology	Sedimentary structures and fossils	Bioturbation and trace fossils	Process interpretation
FA1: Shallow carbonate shelf	Thickly bedded, greenish-white carbonates.	Variety of facies consisting of fossiliferous wackestone, packstone, and grainstone interbedded with dark, bioturbated, pyritic mudstone.	Analysis of carbonate facies is beyond the scope of this paper.	Deposition in a variety of shallow-marine carbonate facies. See, e.g., Bugge et al. (1995) and Ehrenberg et al. (2000) for details.
FA2: Transgressive lag	Well-sorted fine-grained sandstone beds, 20–50 cm thick.	Planar-parallel lamination. In one case: abundant shell fragments.	None observed.	Strong wave-activity. Transgressive lag indicated by change of environment from shallow to deeper below and above.
FA3: Dysoxic shelf	Dark-brown, laminated, silty claystone intervals 25–60 cm thick.	Laminated, sparse organic fragments and abundant pyrite crystals.	Bioturbation generally absent, but sparse horizons with BI4 composed of small elliptical burrows (?Chondrites).	Dark color, pyrite crystals, general absence of bioturbation and lack of sand indicate poor oxygenation (cf. Krumbein and Garrels, 1952) and low energy. Spikes in bioturbation index indicate submarine environment and possible periods of oxygenation (Gani et al., 2005).
FA4: Prodelta turbidites	Thick, laminated, light-gray siltstone with sparse 0.2–10 cm sandstone laminae and beds.	Abundant current ripples, planar lamination and phosphatic nodules. Sandstone beds show indistinct ripples, sharp bases, and occasional flute casts.	BI spiky and varies from 0 to 3. Some levels with abundant Planolites, otherwise low BI.	Phosphatic nodules indicate low depositional rates and relatively high biogenic productivity (cf. Krumbein and Garrels, 1952). Thin turbidites and low trace fossil diversity indicate proximity to riverine input (e.g., Li et al., 2015).
FA5: Turbidite fan	0.1–75 cm sandstone beds interbedded with 0.2–20 cm siltstone beds.	Sandstone beds show normal grading and contain flute casts, massive beds, planar-parallel lamination, current ripples, and overturned bedding. Occasional fluidized beds, dish structures, and basal sand intrusion pipes.	Bioturbation uncommon, sparse horizontal unlined burrows (Planolites) at sandbed tops and mudstone bases.	Interpreted as deposits of sandy turbidites. Lack of wave-generated structures indicates significant water depth (<20–50 m). Sparse bioturbation, thin beds, basal coarsening-upward units and complex variations between sedimentary structures (e.g., Tbcbcd) indicate hyperpycnal (river-fed) rather than surge-type turbidites (cf. Li et al., 2015).
FA6: Wave-agitated shelf	Several-meter-thick greenish-gray mudstone units with sparse 0.2–30-cm-thick sandstone beds and laminae.	Mudstones are laminated, sandstone beds contain common wave ripples, and very rarely upward-fining massive sand beds (turbidites).	BI variable and spiky from BI0 to BI5, but most commonly BI1. Planolites, Teichichnus, and simple vertical burrows common throughout, some intervals with small elliptical burrows (?Chondrites).	Little input of sand and abundant bioturbation indicates a well-oxygenated, normal-salinity, low-energy environment, likely below fair-weather and storm wave base (~20–50 m) and away from fluvial input points (e.g., Li et al., 2015).
FA7: ?Shoreface	Well-sorted fine, uncemented, white sand; beds 2–200 cm thick.	Mostly massive, sparse faint tangential cross-bedding.	None observed.	Confident interpretation impossible. Sedimentary structures and sorting are similar to shorefaces described elsewhere (e.g., Eide et al., 2014, 2015).
FA8: Fluvial channel	Polymict, well-rounded, medium-sphericity conglomerate with coarse sand matrix, 10–>25-cm-thick beds interbedded with medium-grained sandstone.	Poor recovery of this facies, likely due to presence of large clasts causing drilling problems. Planar-parallel lamination and indistinct ripples in sandy intervals.	None observed.	Confident interpretation not possible. Basal erosion surface, rounding of pebbles, and tractional structures in upper part of units indicate fluvial transport of material.
FA9: Tidal flat	Interbedded 1–20 cm rippled sandstone and 0.1–1 cm mudstone beds with flaser and wavy bedding; occasional extraformational clasts.	Desiccation cracks, current ripples, indistinct ripples.	BI 0–1. Arenicolites and simple, vertical burrows are observed.	Rapid variation of energy inferred from variation between sandstone and conglomerate, and mudstone. Presence of Arenicolites and flaser bedding may indicate marine influence and possibly tides.
FA10: Soil	Brick red mudstone, 75 cm thick .	Abundant rhizoliths (root structures), some intensely brecciated intervals.	BI: 6 throughout.	Red color, brecciation, and complete homogenization are interpreted to represent soil formation in arid conditions (cf. Mack and James, 1994).
FA11: Sandy soil	2 m greenish sandstone bed.	Homogenized sandstone with abundant rhizoliths 2–30 mm wide and tens of centimeters long.	BI: 6. No bioturbation or structures observed apart from rhizoliths.	Interpreted to represent soil formation due to surface exposure of sandy deposits over time. Rhizoliths indicate soil formation in semiarid environment (cf. Retallack, 1997).
FA12: Delta front	Interbedded 0.1–5 cm mudstone beds and 0.5–30 cm sandstone beds.	Wave ripples, flute casts, massive, planar-parallel laminated and current-rippled sandstone beds organized in a variety of ways. Thin, normal-graded sandstone beds with flute casts.	BI 0–5, Arenicolites. Diplocraterion, Rhizocorallum, and Planolites are common trace fossils.	Large variation in interpreted energy, dominance of shallow-marine trace fossils, and variation between wave- and current-generated structures indicate shallow-marine conditions, potentially on the delta front (cf. Klausen et al., 2015). Presence of thin turbidites indicates proximity to river mouth (cf. Wellner et al., 2005; Li et al., 2015).
FA13: Tide-influenced channel	Very fine- to sparsely fine-grained sandstone packages several meters thick; sparse 1–10 cm heterolithic interbeds.	Basal erosion surface. Dominance of tangential and trough cross-bedding with single and double mudstone drapes on foresets. Bidirectional current ripples and organic fragments are common. Flaser bedding and planar-parallel bedding common toward top.	BI is commonly 0, sparse mudstone-rich interbeds exhibit up to BI5. Bioturbated intervals consist solely of simple, horizontal, unlined burrows (Planolites?).	Basal erosion surface, dominance of unidirectional paleocurrent indicators, and abundant terrigenous organic matter indicate transport in river channels. Abundant tidal indicators such as single and double mudstone drapes indicate tidal influence. Typical expression of E-derived fluvial systems in the Triassic Barents Sea (cf. Klausen and Mørk, 2014).

Note: Bioturbation index is sensu Taylor and Goldring (1993). BI—bioturbation index. si—silt. Sandstone grain size: vf—very fine, f—fine, m-medium, c—coarse, vc—very coarse. Sy—syneresis cracks. Ta,b,c,d, refer to turbidite divisions (c.f. Walker, 1965), and combinations of letters denote variations within single beds.

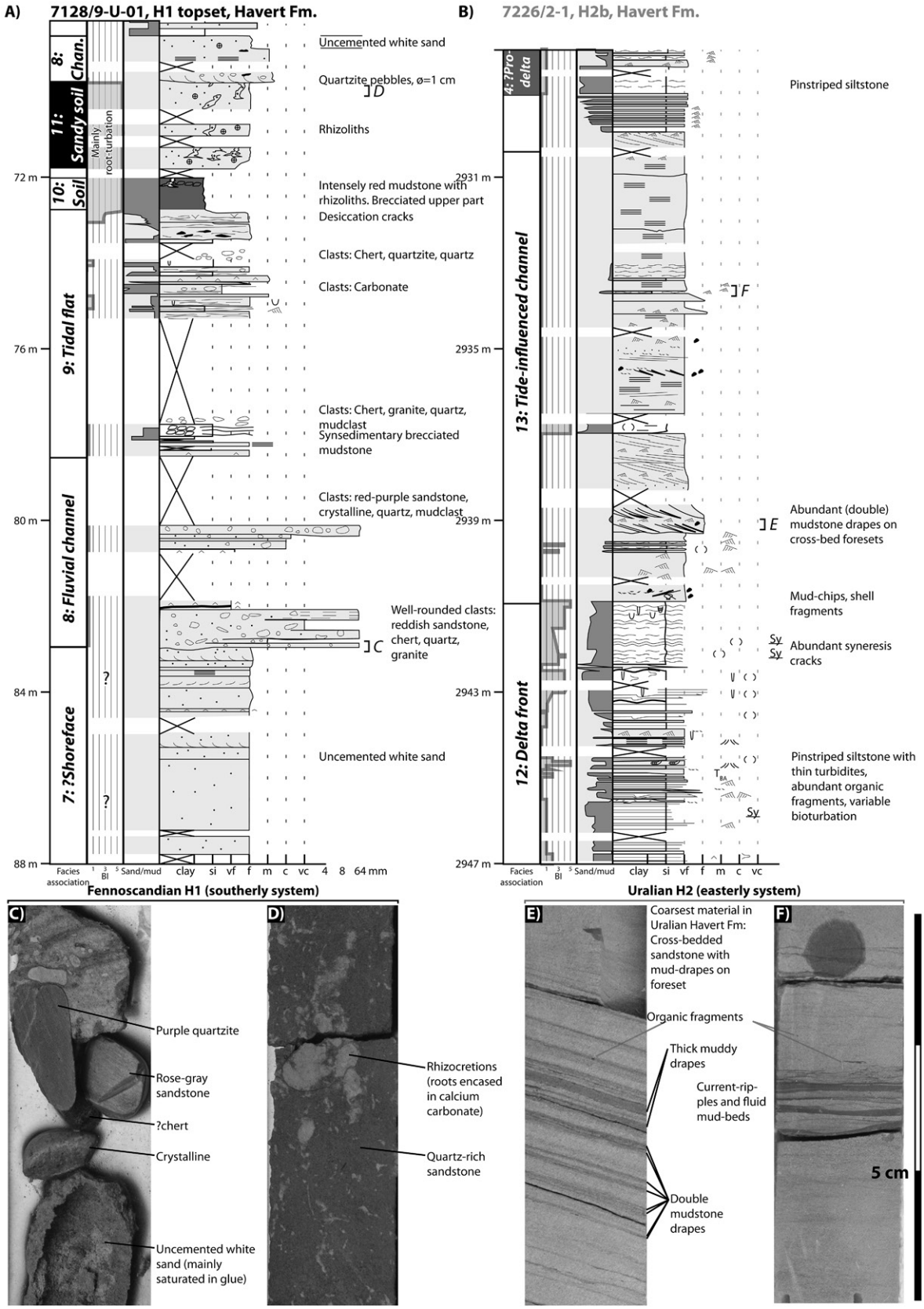

Figure 9 (*Continued on facing page*). Selected core logs and core images from the Havert Formation. BI—bioturbation index, sensu Taylor and Goldring (1993).

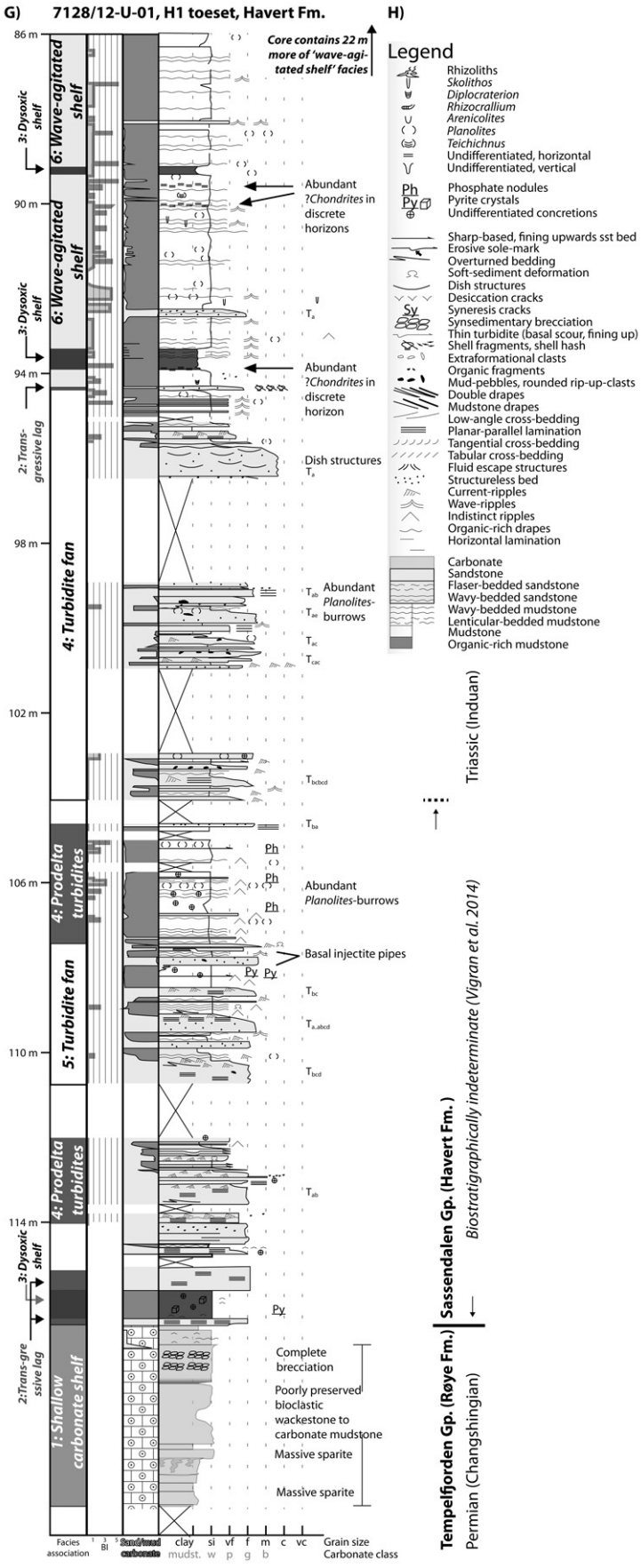

Figure 9 (*Continued*). (A) Typical sandy facies of the H1 interval topset, showing evidence for channels and semiarid paleosols, with several rounded, extraformational clasts. From shallow core 7128/9-U-1. (B) Typical sandy example of topset of the H2b interval of the Havert Formation, from industry well 7226/2-1. Note the fine grain size of the sandstone, which is typical for the entire easterly derived sediment package of the Triassic succession in the Barents Sea. (C) Extraformational conglomerate from the H1 interval topset. (D) Rhizocretions in sandy soil in the H1 interval. (E) Most coarse-grained cored sedimentary rock in the H2 interval in the Barents Sea, consisting of cross-bedded fine-grained sandstone with abundant mudstone drapes. (F) Typical sandy facies of the H2 interval. Positions of C–F are indicated in the core descriptions. (G) Log showing typical development of the Permian Røye Formation of the Tempelfjorden Group, the boundary to the Havert Formation, which approximates the Permian-Triassic transition, and typical development of the H1 bottomset and clinoforms. From shallow core 7128/12-U-01. sst—sandstone; si—silt. Sandstone grain size: vf—very fine, f—fine, m-medium, c—coarse, vc—very coarse. Sy—syneresis cracks. $T_{a,b,c,d}$, refer to turbidite divisions (c.f. Walker, 1965), and combinations of letters denote variations within single beds.

fine-grained to rarely fine-grained sandstone beds with cross-beds, in many cases with single and double mudstone drapes (Figs. 9E–9F), interpreted as the deposits of tide-influenced distributary channels. Along with widespread shelf deposits, this is similar to the depositional environments described in the remainder of the Uralian-derived Triassic succession in the Barents Sea (e.g., Mørk and Elvebakk, 1999; Bugge et al., 2002; Klausen and Mørk, 2014).

Mineralogical Data

The difference between the H1 interval and the majority of the remainder of the Triassic succession in the Barents Sea, including the H2 interval, is further illustrated by the petrological work performed by Mørk (1999). Primarily, the majority of the Uralian-derived systems consist of very fine-grained lithic arkoses with roughly equal amounts of quartz, feldspar, and lithic fragments, which yield unfavorable hydrocarbon reservoirs after diagenesis (Fig. 10). This is mainly due to the young, volcanic nature of the Uralian and Kara sediment sources, and a long transport distance, leading to extraction of coarse material (Omma, 2009; Pózer Bue and Andresen, 2014).

Conversely, the Fennoscandian-derived deposits of the H1 interval consist of quartz arkose, and they preserve porosity to a much higher degree (Fig. 10). The conglomeratic clasts in the H1 interval consist of sandstone, chert, quartz, granite, and carbonate, ordered by upward-decreasing frequency in the core (cf. Fig. 9C). The sandstone clasts are fine grained and deep-red, purple, and pink (Fig. 10D), and they are similar to the mineralogically supermature, late Neoproterozoic deposits onshore Finnmark in northern Norway (cf. Fjellanger et al., 2006; Nystuen, 2008). The granite clasts also indicate a shield affinity, strongly suggesting these sediments were derived from northern Norway.

Paleocurrent Directions and Thickness Trends

As shown already, the H1 interval consists of a relatively linear system stretching from Troms to the Kola Peninsula, and it exhibits a large protrusion interpreted as a major delta located just offshore the present-day Tanafjord (Fig. 2). The center of the Tana fan of the H1 interval is directly offshore the present-day Tanafjord (Fig. 11). Furthermore, paleocurrents in the Tana fan (measured from slightly arcuate clinoforms, a turbidite fan, and river channels imaged in amplitude maps) all show paleocurrents away from the mouth of the present-day Tanafjord (Figs. 7D and 11). Thus, if these

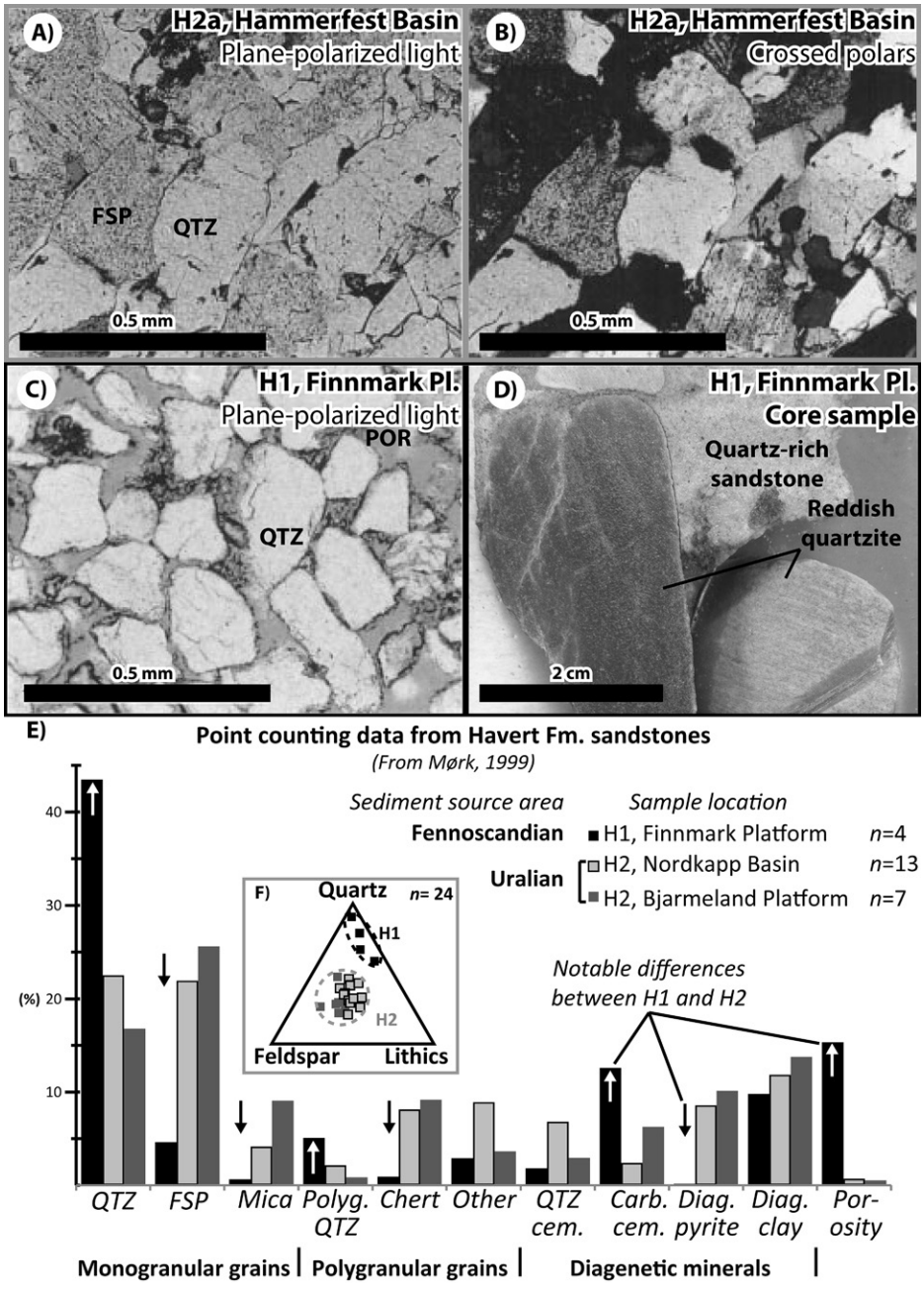

Figure 10. Petrological data from Havert Formation sandstones, highlighting the difference between the Uralian (grays) and Fennoscandian (black) source areas. Data were compiled from Mørk (1999). (A) Thin section of typical sandstone from the easterly derived deposits. Note the low porosity (epoxy, homogeneous) and the high feldspar (Fsp) content. (B) A with crossed polarizers. (C) Thin section of typical Fennoscandian-derived sandstone of the Havert Formation from the Finnmark Platform. Note the high quartz-content (Qtz) and porosity (POR, epoxy), and the angular shape of grains. (D) Core photograph from sandstone from the Tana fan of the H1 interval on the Finnmark Platform. Note rounded, reddish quartzite pebbles. (E) Class-averaged point-counting data from the Havert Formation. Note the similarity of the Uralian deposits from different areas (gray colors) and the striking difference between the Uralian and Fennoscandian deposits (black). (F) Quartz-feldspar-lithics (QFL) plot of point-counting data showing domains of the two populations. A–C are from Mørk (1999). QTZ—quartz; FSP—feldspar; POR—porosity; Polyg—polygranular; cem—cement; Diag—diagenetic.

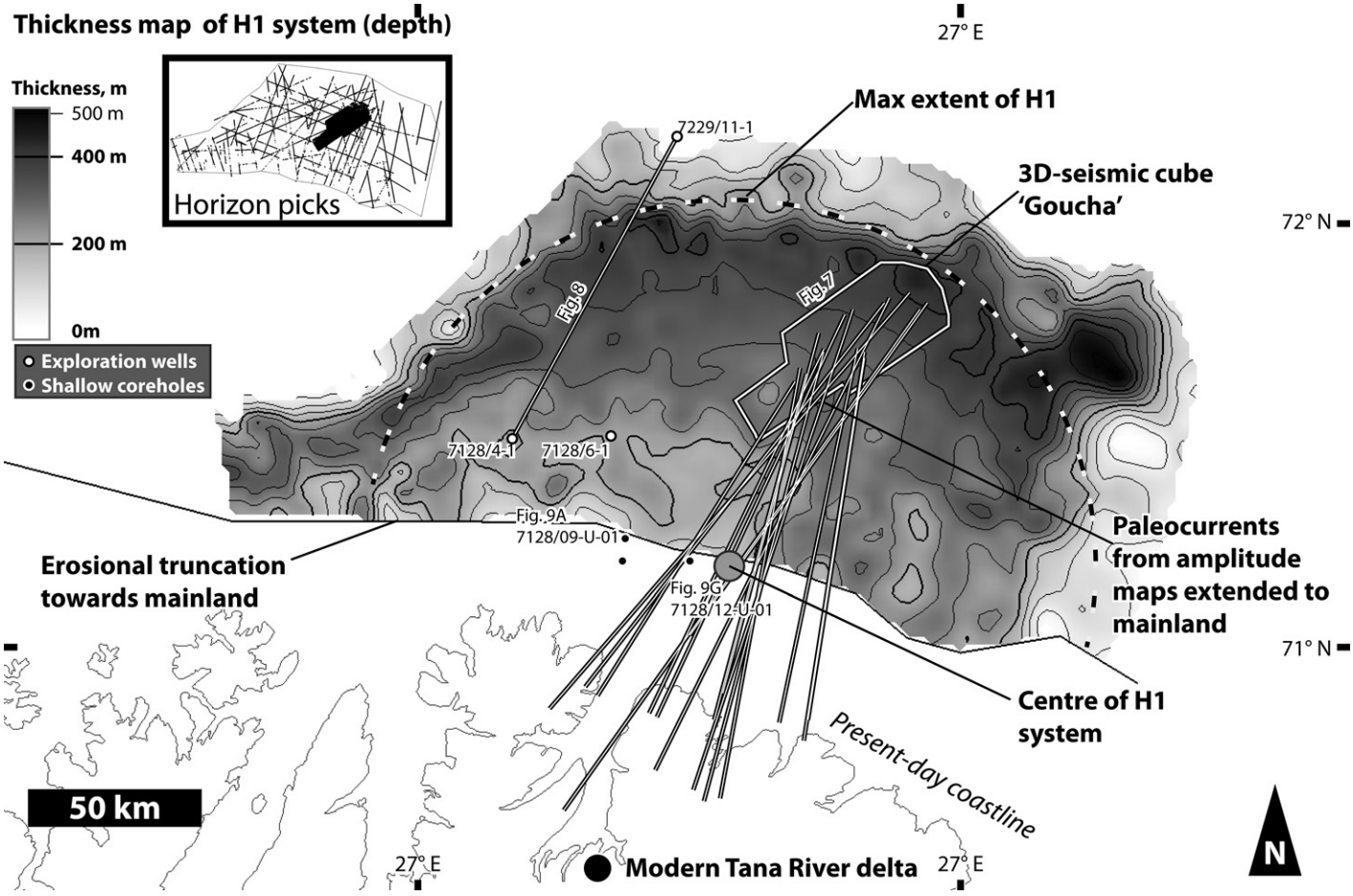

Figure 11. Depth-converted thickness map of the Tana fan of the H1 interval of the Havert Formation near Tanafjord. Note that the fan has a semicircular shape with center located just off the mouth of the present-day Tanafjord, and that paleocurrent measurements extrapolated from the three-dimensional (3D) seismic cube point away from the mouth of the present-day Tanafjord (cf. Fig. 7D).

are projected backward toward the mainland, they indicate sediment transport from the area around the present-day Tanafjord. This strongly suggests that the sediment in the H1 Tana fan was supplied through a fan apex located near the mouth of the present-day Tanafjord, and that Tanafjord has acted as a long-lived sediment input point.

Shoreline trajectories in the H1 interval are relatively flat, with little evidence of aggradation in the clinoform package (Figs. 5 and 7A). This indicates high sediment supply and relatively stable sea level. The H1 interval increases in thickness basinward, which could be mainly due to progradation into a basin with basinward-increasing water depth, or due to much less subsidence generation near the basin margin during deposition. If a linear thickness decrease is assumed past the eroded area (i.e., south of the subcrop line), the extrapolated thickness reaches zero around the innermost fault of the Austhavet fault zone (cf. Fig. 4). This supports the interpretation of the present-day coast and nearby Finnmark fault as a long-lived hinge zone between the Barents Sea Basin and the Fennoscandian Shield. Furthermore, it may thus be speculated that the apex of the sedimentary system was located close to the Austhavet fault zone.

Summary and Mass Balance

The H1 interval of the Havert Formation consists of a sedimentary system sourced from northern Fennoscandia, and it is mineralogically and sedimentologically distinct from the later systems that prograded into the western Barents Sea from the Uralian foreland basin and Kara Sea during the Triassic. A large delta system in the H1 interval prograded from NW Norway (Fig. 2) and is interpreted to have had a fan apex (i.e., sediment entry) point close to the mouth of Tanafjord (Fig. 11).

The entire volume of the preserved part of the Tana fan of the H1 interval off Tanafjord was obtained by interpretation of the available seismic lines (Fig. 11). The resulting isochore map was depth converted using velocity-depth curves derived from sonic logs in available wells and shallow core holes (Fig. 8; Bugge et al., 1995) and later converted into mass using relevant density log measurements from wells (Fig. 8) and a depth-density relationship based on these measurements. This yielded a mass of 1.4×10^{16} kg for the preserved parts of the Tana fan of the H1 interval. However, part of this fan was removed by later erosion. If the Tana fan of the H1 interval is assumed to have thinned linearly toward the Austhavet fault zone, which appears reasonable from the seismic data and thickness map (Figs. 4 and 11), an additional mass of 5.7×10^{14} appears to have been removed through postdepositional erosion, yielding a reconstructed mass

of 1.46×10^{16} kg (4% greater than the unrestored mass).

In order to compare this number to modern systems (cf. Milliman and Farnsworth, 2011), it must be converted into sediment load (average mass of sediment supplied through the fan apex annually). To estimate the sediment load of the Tana fan of the H1 interval, a time-model must be established. This is not straightforward, as the top of the H1 interval has not been cored and is therefore not biostratigraphically dated. However, the Induan stage is particularly well dated (Ogg et al., 2014), also in the Barents Sea (Vigran et al., 2014). The H1 interval makes up 25% of the thickness of the Havert Formation in wells 7128/4-1 and 7128/6-1, the only wells penetrating the entire Havert Formation on the Finnmark Platform, and the Havert Formation spans the Induan Stage. Assuming gradual subsidence throughout the Induan Stage, and considering that the Induan Stage lasted 2.2 m.y. (Gradstein et al., 2012; Ogg et al., 2014), we estimate that deposition of the H1 interval took 0.54 m.y., which yields a sediment supply of 27 MT/yr through the apex of the Tana fan of the H1 interval. These estimates are of course uncertain, but they serve as a first-order approximation based on the available data.

This estimate assumes balance between mass extracted and mass introduced by longshore drift, hyperpycnal plumes from other delta systems, and wind. These assumptions appear to be reasonable because: (1) the toesets of the H1 unit are very thin, which indicates negligible hemipelagic sedimentation, and negligible eolian and hyperpycnal plume transport of sediment sourced from other delta systems into the studied parts of the basin (Figs. 4, 5, and 7A), and (2) strongly wave-influenced deposits are only very sparsely observed in the Barents Sea Basin during the Triassic (Klausen et al., 2016), which indicates a low potential for significant transport of sediment through longshore drift.

The calculated values are similar to modern rivers draining the Indian craton, such as the Brahmani, Mahanadi, and Godavari Rivers, which have sediment loads of ~30–60 MT/yr (Milliman and Farnsworth, 2011). Worldwide, modern continental-scale and/or orogenic-scale river systems, such as the Amazon, Ganges, Brahmaputra, and Mississippi Rivers, have sediments loads in the order of 200–1200 MT/yr, and modern small rivers draining low-gradient catchments and hard lithologies have very low (<5 MT/yr) sediment loads. This analogue to midscale rivers draining shield rocks will be investigated later herein by undertaking a geomorphological study of the present-day uplands onshore of the Tana fan, and by utilizing the BQART model to estimate mass balances (Syvitski and Milliman, 2007).

GEOMORPHOLOGY OF NORTHERN FENNOSCANDIA AND THE MODERN TANA RIVER CATCHMENT

Several onshore geomorphological features have been interpreted as remnants of long-lived catchments in Fennoscandia. Some examples are the Porsangerfjorden in the Carboniferous of northern Norway (Bugge et al., 1995; Roberts and Lippard, 2005); the Jurassic Sognefjord–-Troll Field system (Nesje and Whillans, 1994; Sømme et al., 2013); the latest Cretaceous to earliest Paleogene Romsdalsfjorden-Ormen-Lange system (Sømme et al., 2009b); the Mesozoic Norwegian strandflat and high-altitude plateaus (Lidmar-Bergström et al., 2013; Olesen et al., 2013) in western Norway; and several geomorphic features in Sweden (e.g., Lidmar-Bergström et al., 2013). Many examples also exist worldwide (e.g., Cretaceous to present-day Gulf of Guinea; Leturmy et al., 2003). In order to investigate the potential for preservation of elements that may have been part of the H1 catchment within the present-day landscape in northern Fennoscandia, an assessment of the present-day geomorphology must be performed. Hence, it is also important to consider the effects of glacial modification from the Quaternary and late Neogene ice sheets.

On a large scale, the northern Fennoscandian landscape today consists of three domains (Fig. 2A): (1) The Atlantic coast is dominated by coastal mountains, which are dissected by several fjords. (2) East of the coastal topographic maximum, the landscape is dominated by a gentle regional slope toward the Gulf of Bothnia in the SE. (3) The Barents Sea coast and hinterland are dominated by low slopes and large lakes with drainage toward the north (Figs. 2A and 12A).

A 400-m-deep coast-parallel trough occurs offshore along the northern Norwegian coast, originating from the mouths of the Pasvik and Tuloma Rivers, and it is fed into by the nearby fjords (Fig. 12; Winsborrow et al., 2010). This is an area of maximum erosion by topographically controlled ice streams (Laberg et al., 2012). Block-field–mantled high-altitude plateaus occur particularly in the Varanger Peninsula (Fig. 12A), indicating that the plateaus were overlain by cold-based glaciers and largely escaped glacial erosion (Fjellanger et al., 2006). Landscapes without U-shaped valleys and streamlined inselbergs are common away from the coast and high mountains in NW Fennoscandia, something which indicates negligible glacial erosion (cf. Ebert et al., 2015).

The regional drainage divide between the Norwegian Atlantic coast and the Gulf of Bothnia coincides with the coastal topographic maximum as far north as Troms (Fig. 2A). In Troms, the drainage divide turns inland and coincides with a linear, gentle high between Troms and the Kandalaksha Gulf. The coastal catchments south of Troms are small, short, and steep. However, the Reisa, Alta, and Tana Rivers near the bend in the drainage divide are deeply incised into bedrock and drain areas up to 250 km south of the topographic maximum (Fig. 2A). Further to the east, in catchments such as the Pasvik and Tuloma, the catchments are larger and flatter and contain large lakes (Figs. 2A and 12A). These also show abundant evidence of glacial erosion (Fig. 12C), such as streamlined inselbergs and overdeepened lakes.

The majority of the area in northern Norway and Finland is drained by the Tana and Alta Rivers (Fig. 2A). The intervening fjords, Porsangerfjord and Laksefjord, are only connected to insignificant coastal catchments (Fig. 2A).

Since there are several lines of evidence suggesting that the earliest Triassic Tana fan of the H1 interval had its apex located close to the mouth of the present-day Tanafjord, we investigated the geomorphology of the present-day Tanafjord, Tana River catchment, and surrounding landscape in northern Norway and Sweden. The Tana River clearly shows antecedent features: The river is deeply incised into a regional bedrock plain that is tilted toward the SE, opposite to the drainage direction of the river; the drainage is strongly asymmetric, as tributaries from the SW are consistently larger than those from the SE; and it is incised into topographic highs instead of being deflected (Fig. 12A; Gjessing, 1978). Furthermore, the river is clearly incised up to several hundreds of meters into a regional etch surface (sensu Ebert, 2009), and it strongly conforms to the fracture pattern of this surface, resulting in a strongly rectangular drainage pattern (Fig. 12B). No alignment to glacial pathways is observed. This is in strong contrast to surrounding areas modified by Quaternary ice streams, such as in the Pasvik catchment, which shows abundant streamlined inselbergs and glacially overdeepened lakes (Fig. 12A).

This indicates that the river channel geometry of the Tana River is mainly preglacial. The river is markedly asymmetric, with tributaries from the west draining larger areas than tributaries from the east. However, some of the easterly tributaries are very large compared to the area they are draining, particularly the Polmok tributary (Fig. 12A). The catchments directly to the east of the Tana River catchment have large and abundant lakes (e.g., Lake Inari) and well-developed

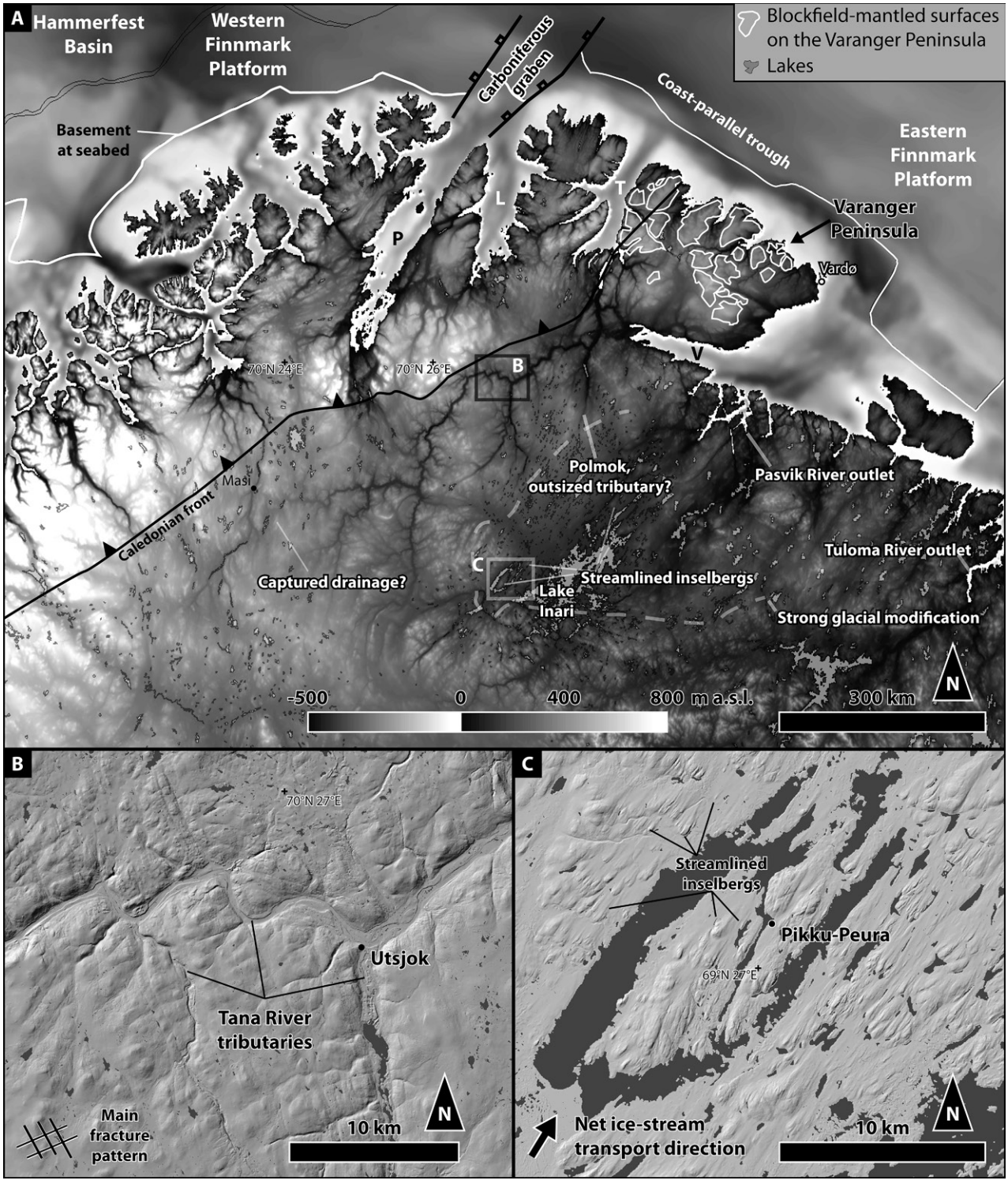

Figure 12. (A) Topography and bathymetry of NW Fennoscandia. Note the rectangular tributary pattern of the Tana River (under rectangle showing location of part B), the outsized Polmok distributary, and the strongly glacially modified areas around Lake Inari, which are part of the Pasvik River catchment. A—Altafjorden; P—Porsangerfjorden; L—Laksefjorden; T—Tanafjorden; V—Varangerfjorden. (B) Hillshade map of the area around Utsjok, highlighting an area with negligible glacial modification. Note that the river pattern is strongly rectangular and corresponds to the well-developed bedrock fracture pattern. See part A for location. (C) Hillshade map of the area around Pikku-Peura, highlighting an area with strong glacial modification. Note the large amount of streamlined inselbergs aligned with the regional ice-stream transport direction, abundance of overdeepened, ice-stream–aligned lakes, and lack of any pronounced bedrock-derived topographic features. See part A for location.

streamlined inselbergs (Fig. 12C), and drain toward the coast-parallel trough. We thus speculate that the Polmok tributary was connected to a larger catchment prior to glaciation, but that parts of this catchment were modified by glacial erosion and later incorporated into the Pasvik catchment (cf. Fig. 2A).

The uppermost tributaries in the Alta catchment resemble the uppermost tributaries in the Tana catchment. These may be speculated to have drained toward the Tana earlier and later were captured by the steeper Alta River. Thus, the low valley SE of Masi may represent a cutoff tributary of the Tana River. The lack of larger protrusions in the Induan sedimentary systems in front of the currently large Alta and Pasvik catchments may be due to the fact that these catchments were much smaller during the Early Triassic than they are today.

In sum, these observations support that the Tana catchment geometry was developed prior to the Quaternary glaciations, and that its present form has experienced minor glacial erosion, but that the catchment may have been larger prior to the Quaternary glaciations due evidence of glacial modifications of the eastern and coastal parts and possible river capture in the west. The close association with sedimentary geometries in the H1 interval suggests that the Tana catchment and at least parts of the catchment geomorphology had already developed in the Triassic.

MASS-BALANCE CALCULATION

Model and Variables

To test how the present-day catchment of the Tana River could have related to the catchment for the Induan Tana fan of the H1 interval, a mass balance of the Tana fan source-to-sink system was investigated. Based on an analysis of hundreds of modern systems, Syvitski and Milliman (2007) devised an empirical model for mass transport from catchments to the ocean. In catchments with annual average temperatures greater than 2 °C, unaffected by glaciers or humans, this model may be formulated as:

$$Q_s = \omega L Q_w^{0.31} A^{0.5} R T, \quad (1)$$

where Q_s is sediment discharge (10^6 t/yr), ω is an empirical constant (ω = 0.0006), L is a variable for bedrock erodibility (with extremes of 0.5 to 3 for hard metamorphic/plutonic bedrock and erodible loess, respectively), Q_w is annual water discharge (km^3/yr), A is catchment area (km^2), R is maximum catchment relief (km), and T is long-term basin-averaged temperature (°C; for further discussion of the individual parameters, see Syvitski and Milliman, 2007). For the H1 system, the different factors were estimated as follows:

Q_s: Sediment Supply

The annual sediment supply through the Tana fan apex was estimated to be 27 MT/yr, based on the observations and assumptions made in the section on "Paleocurrent Directions and Thickness Trends."

L: Lithology

Based on the compositions of clasts observed in core, which consisted of a majority of well-cemented sandstone clasts resembling known outcrops of Neoproterozoic sandstone and subordinate amounts of crystalline shield rocks, we interpreted the majority of the catchment to have consisted of sedimentary rocks. This is consistent with results from fission-track data (Larson et al., 1999, 2006; Hendriks and Andriessen, 2002), which indicate a sedimentary cover related to a Caledonian foreland basin to have been present on the Fennoscandian Shield during the latest Permian and Early Triassic. The preferred value for L is therefore 2 (clastic sedimentary rocks).

R: Relief

Estimation of relief in an eroded catchment is difficult. However, maximum relief in a region is mainly a function of the large-scale tectonic setting. The study area was adjacent to the nonvolcanic rift between Norway and Greenland in the latest Permian and Early Triassic (e.g., Ziegler, 1992; Stoker et al., 2016). In the present, areas close to nonvolcanic rifts such as the Red Sea rift, or the nonvolcanic parts of the East African rift, show a maximum topography close to 3 km due to dynamic rift shoulder uplift (Wernicke, 1985; Daradich et al., 2003). Since the H1 catchment might not have drained the very peaks of the rift flanks, a preferred value for maximum relief of 2 km was chosen. However, since this is a difficult parameter to estimate, calculations were performed with different relief values spanning 1–5 km (Fig. 13).

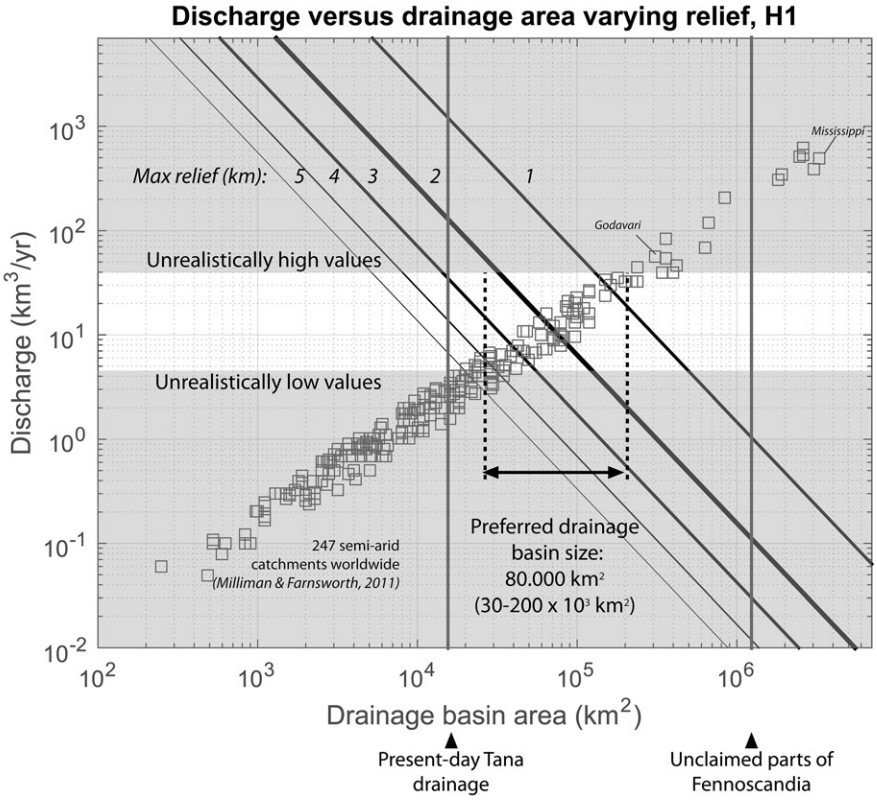

Figure 13. Estimation of catchment size for the Tana fan of the H1 interval using the BQART model (Syvitski and Milliman, 2007). Solid lines show calculated relationships for different values of catchment relief during the Triassic (preferred relief: 2 km). Red rectangles show discharge and drainage basin area for 247 modern, semiarid catchments worldwide (data points from Milliman and Farnsworth, 2011).

T: Temperature

Several studies have investigated the paleoclimate of the Early Triassic, and Péron et al. (2005) estimated the yearly average temperature at the northern margin of Fennoscandia to be ~20 °C during the Olenekian, which is a period with global temperatures similar to what is estimated for the Induan and consistent with low latitudinal temperature variation during the Early Triassic (Sun et al., 2012).

Q_w: Water Discharge

Water discharge is a function of drainage basin size and climate (rainfall, evapotranspiration, and runoff efficiency). It is notoriously difficult to estimate in ancient systems, but in modern systems, a relatively clear power-law relationship exists between discharge and catchment area for different climatic zones (Fig. 13; see also Milliman and Farnsworth, 2011).

Several studies have shown that the climate in Fennoscandia and the Barents Sea Basin was semiarid during the Induan (Chumakov and Zharkov, 2003; Péron et al., 2005; Nystuen et al., 2014). This agrees well with the observations of a deep-red paleosol with rhizocretions in core data in this study (Fig. 9S). Discharge therefore was not estimated by a single value, but it was taken as an unknown that varied with the other unknown, which is the catchment area. These two variables were estimated by plotting discharge and drainage basin area for 247 semiarid catchments worldwide (Fig. 13), derived from the database of Milliman and Farnsworth (2011).

A: Catchment Area

Defining the size of the H1 catchment is the objective of the mass-balance study. Some bounds may be put on the extent of the drainage basin prior to calculations (cf. Fig. 1): Significant amounts of sediment were delivered from Fennoscandia to rift basins both in the North Sea (McKie and Williams, 2009; Nystuen et al., 2014) and Norwegian Sea (Müller et al., 2005) during latest Permian–Early Triassic rifting along the W and SW margins of the Norwegian mainland. Rifting probably led to development of a topographic axis along the rift flank (cf. Gawthorpe and Leeder, 2000), which likely acted as a westernmost possible drainage divide for the Tana River. The Ural foreland is an easternmost boundary, and a southern margin extending almost to the south of Sweden is an absolute maximum, due to the presence of the North German Basin and Polish Trough to the south (Fig. 1; e.g., Geluk, 2005; McKie and Williams, 2009). This yields a maximum drainage area of 1.3×10^6 km^2. For reference, the area of the present-day Tana catchment is 16×10^3 km^2 (Fig. 13).

Calculation Results

Using the chosen variables as input, and keeping the water discharge and catchment area as unknowns, the calculations yielded the relationships plotted in Figure 13. The relationships are plotted together with discharge and area for 247 semiarid (runoff: 100–250 mm km^{-1} yr^{-1}) catchments worldwide from Milliman and Farnsworth (2011). The intersection between the calculated relationships and the area-discharge values for modern systems indicates that a catchment for the H1 interval spanning the majority of Fennoscandia is unlikely. Similarly, catchment areas in the same size as the present-day Tana River catchment would not likely be able to generate sufficient sediment within the available time span. The model indicates a preferred catchment size of 80×10^3 km^2, with a range of 30×10^3 to 200×10^3 km^2.

The preferred catchment area for the Tana fan of the H1 interval is 5 times larger than the present-day Tana River catchment. However, as discussed earlier herein, this catchment has likely been modified and made smaller since the Early Triassic by the development of coast-normal glacial fjords, and possibly by glacial modification to the east and river capture in the west. If the glacier-modified coastal parts just seaward of the present-day Tana River catchment, the uppermost reaches of the present Alta River catchment, and eastern parts of the Pasvik catchment are added to the Tana River catchment (cf. Figs. 2 and 12), this yields an area of 60×10^3 km^2, which is comparable to the calculated catchment area for the H1 system. Extension of the catchment south of the present-day regional drainage divide is thus not required by the data or models.

DISCUSSION

Uncertainty of Catchment Size Estimates

The estimated size of the catchment of the Tana fan of the H1 interval during the Induan Stage is critical to understand how this catchment may have related to present-day topography, and to estimate denudation during the Triassic. The uncertainty of this estimate is therefore considered here. Varying the estimate for paleotopography within realistic bounds of 1–5 km does not significantly change the outcome of the estimates from the BQUART model presented earlier herein: The catchment size is still estimated to be significantly larger than the present-day Tana River, and smaller than the majority of Fennoscandia (Fig. 13). Varying the temperature within reasonable bounds (±5 °C) changes the estimated catchment area by a factor of 2, which is insignificant compared to the uncertainty. Considering the large uncertainties for these estimates, constraining paleotemperature further would thus not significantly decrease the uncertainty of the estimates. Varying the lithology coefficient L to correspond to high-grade metamorphic and plutonic basement increases the estimated catchment size by a factor of 10, but this is not realistic based on the present-day bedrock, which mainly consists of sedimentary and hard but mixed lithologies (e.g., Sigmond, 1992). The present-day lithology is likely to be harder and less erodible than what it was during the Early Triassic due to continued net erosion of the catchment. The estimate that would benefit the most from better constraints is therefore considered to be the catchment lithology. This could be improved through provenance analysis of the H1 system.

Mechanism for Sudden Sediment Influx after the Permian-Triassic Transition

A sharp increase in sedimentation rates and clay content immediately after the Permian-Triassic transition has been noted close to continental margins all over the world, and it is generally attributed to a climate-driven increase in weathering and destruction of terrestrial ecosystems (Algeo and Twitchett, 2010). Increased sediment supply is also recognized in the Barents Sea Basin at this time (Fig. 3C), not only from Fennoscandia along the northern margin (this study), but also from Greenland to Spitsbergen (e.g., Wignall et al., 1998), and from the Kara Sea and the Urals to the greater Barents Sea Basin (e.g., Puchkov, 2009; Glørstad-Clark et al., 2010). In the Barents Sea, however, the increased influx not only indicates an increase of fine-grained sediment, but also the progradation of sandy delta systems for tens of kilometers and transport of conglomerates into the proximal parts of the basin. It is hard to explain this large increase in sediment influx simply by ecosystem collapse and increased weathering. A possible explanation for the sudden influx close to Fennoscandia and Greenland is tectonic uplift associated with rifting along the Norway-Greenland margin (e.g., Müller et al., 2005), possibly in the form of rift shoulder uplift. The progradation of the large, Uralian-derived easterly system was likely related to tectonism coincident with and caused by the main phase of volcanism of the Siberian Traps (Burgess and Bowring, 2015), as the Uralian orogeny was in a waning phase at this stage (Puchkov, 2009). This likely led to large-scale uplift and erosion of the Uralian

orogen, and to vastly increased sediment supply in the Early Triassic and deposition of coarse-grained fluvial deposits in the Uralian foreland basin (Puchkov, 2009; Reichow et al., 2009).

Catchment Reorganization at Permian-Triassic Boundary

The Tanafjord is the largest catchment in northern Norway today, and it appears that the Tana catchment was even more dominant during the Triassic (cf. Fig. 13). However, the catchments in northern Fennoscandia were significantly different during pre-Triassic times: During the Visean (Carboniferous), a major delta system prograded from a SW-NE–oriented graben structure that coincides with the present-day Porsangerfjorden (Figs. 2 and 12; Bugge et al., 1995; Roberts and Lippard, 2005). The mouth of this fjord was not associated with a pronounced sediment input point during the Triassic, and there are only insignificant catchments discharging into the Porsangerfjorden today (Figs. 2 and 12). In general, Paleozoic structures (cf. Gudlaugsson et al., 1998) do not appear to have exerted any influence on the present-day nor Triassic catchment geometry in northern Norway, and the organization of the present-day catchments is similar to what it was in the Triassic (cf. Fig. 12). This suggests that the present-day catchment organization in northern Norway was established during the onset of Late Permian and Early Triassic rifting in northern Fennoscandia. This rift episode likely led to abandonment of the older, Carboniferous drainage pattern, and a complete reorganization of catchments. These results highlight the potential longevity of catchments through geological time, and the potential of extensive catchment reorganization to occur during significant regional tectonic events such as onset of rifting.

Denudation Rates in H1 Catchment

Assuming a sediment source for the Tana fan of the H1 interval consisting of sedimentary rock, a rock density of 2.2 g/cm^3 in the sediment source region, a catchment size of 80 × 10^3 km^2 (Fig. 13), and using the sediment mass calculated for the Tana fan of the H1 interval above, the interpretations presented here indicate erosion of 90 m of rock in the catchment area during deposition of the H1 interval (with a range of 230–35 m for the smallest and largest catchments estimated above). Applying the time model devised in the section "Paleocurrent-Directions and Thickness-Trends," this yields a denudation rate of 0.15 km/m.y. This is similar to denudation rates measured at long time scales in mountainous catchments (Kirchner et al., 2001; von Blanckenburg, 2005), indicating that these estimates are reasonable.

If the calculated denudation rate for the H1 interval was stable over the entire Triassic, this would lead to denudation of ~8 km in the catchment. This is clearly incompatible with fission-track data, which indicate minor denudation in NW Norway since 300–250 Ma (Hendriks and Andriessen, 2002; Hendriks et al., 2007). Therefore, sustained high denudation rates through the Triassic in the catchment of the Tana fan of the H1 interval are deemed as unrealistic. There is also no seismic evidence of later prograding, southerly derived clinoforms or fluvial channels in the Triassic Barents Sea (Fig. 4; Glørstad-Clark et al., 2010; Klausen et al., 2015). However, petrological data from the SW Barents Sea indicate more mineralogically mature sands with higher Sm/Nd ages close to the Fennoscandian Shield for at least the entire Early and Middle Triassic (Mørk, 1999).

In sum, this indicates that NW Fennoscandia was subject to tectonic activity around the Permian-Triassic transition and produced large amounts of sediment during this time. It is likely that the system had been transport-limited during most of the Permian and late Carboniferous, when the Barents Sea was an evaporate basin and later a carbonate platform (e.g., Worsley, 2008), and that some of the decline in sediment supply and denudation rates was related to depletion of stored weathered material. Subsequently, in the late Induan and at least until the end of the Middle Triassic, weathering and sediment transport continued, albeit at a lower rate. This indicates that the Fennoscandian source area was not buried by Triassic sediments or shut down, but continued to supply sediment to the basin throughout the Triassic.

Importance for Reservoir Characterization

This study shows how source-to-sink estimates can be applied to predict the distribution of high-quality reservoir rocks in ancient sedimentary basins. In basins with multiple sediment input points with distinct sand populations, it is important to constrain the relative importance of the different catchment areas and their potential to deliver sand. These factors will be determined primarily by relief, climate (water discharge and temperature), bedrock type, and catchment area (Syvitski and Milliman, 2007) and will have a first-order control on the distribution of reservoir quality in the basin.

For example, as the reservoir properties of easterly derived sand in the Triassic Barents Sea strata are poor, this study shows that potential reservoirs will have greater quality along the basin margins (Fig. 10). This is true both for the Induan H1 interval, but also for the remainder of the Triassic succession (Mørk, 1999). As the Fennoscandian sediment source was emergent and continued to supply sediment throughout the Triassic, albeit at a reduced rate compared to the Induan, mixing of the Fennoscandian and Uralian sand types near the basin margin would have occurred. This would lead to consistently better reservoir quality closer to the craton. This is to be expected in other systems where vast axial fluvial systems are supplying immature sediments, and smaller, contributory systems are supplying more mature sediments.

CONCLUSIONS

An Early Triassic point-sourced sedimentary system (the Tana fan of the H1 interval) prograding into the SW Barents Sea has been constrained using seismic, well, core, and petrologic data, and it can be tied to antecedent topography in the source area. This succession consists mainly of southerly shield-derived sedimentary rock, and it contains large amounts of mature sandstone. This is in contrast to the vast fluvio-deltaic sedimentary system sourced from the Uralian orogen and present-day Kara Sea in the east that makes up the majority of the basin fill, which contains immature sandstones and large amounts of mudstone. Sedimentary geometries indicate that the southerly system, the Tana fan of the H1 interval, was sourced from a catchment near the present-day Tanafjord, and that the present-day Tana River catchment has preserved several geomorphic features developed around to the Permian-Triassic transition.

Mass-balance models used to constrain catchment geometries give robust results and, together with petrological data, indicate that the sudden progradation of the H1 interval was related to tectonic uplift caused by the latest Permian–earliest Triassic rift episode, possibly combined with large amounts of stored material weathered during the Permian. After the early Induan, estimates suggest that Fennoscandia continued as a sediment source, but at a smaller rate than before, depositing sandstones with comparatively better reservoir properties than Uralian-sourced sandstones along the margins of Fennoscandia.

This study highlights how source-to-sink methods can be applied to better understand and constrain landscapes and sedimentary systems as far back as the early Mesozoic, and it shows how investigation of source-to-sink relationships in sedimentary systems can increase predictability in hydrocarbon exploration. It also highlights the possibility of preservation of sediment-routing systems and ancient catchment geometries through extended periods of

geologic time, and that extensive catchment reorganization can occur during regional tectonic events.

ACKNOWLEDGMENTS

We thank reviewers Bjørn Anders Lundschien and Atle Mørk for the considerate and careful reviews, which improved this paper, and Associate Editor Henning Dypvik and Editor Aaron Cavosie for their editorial guidance and good suggestions. This work was funded by the Trias North project under grant 234152 from the Research Council of Norway (RCN), along with financial support from Tullow Oil Norge, Lundin Norway, Statoil Petroleum, Edison Norge, and Dea Norge. Mai Britt E. Mørk and Reidar Müller are acknowledged for important discussions and access to data. We are also grateful to Tony Doré, who read an earlier version of the manuscript and provided insightful comments. TGS-Nopec is thanked for allowing us to publish seismic data.

REFERENCES CITED

Algeo, T.J., and Twitchett, R.J., 2010, Anomalous Early Triassic sediment fluxes due to elevated weathering rates and their biological consequences: Geology, v. 38, no. 11, p. 1023–1026, doi:10.1130/G31203.1.

Baig, I., Faleide, J.I., Jahren, J., and Mondol, N.H., 2016, Cenozoic exhumation on the southwestern Barents Shelf: Estimates and uncertainties constrained from compaction and thermal maturity analyses: Marine and Petroleum Geology, v. 73, p. 105–130, doi:10.1016/j.marpetgeo.2016.02.024.

Bergan, M., and Knarud, R., 1993, Apparent changes in clastic mineralogy of the Triassic-Jurassic succession, Norwegian Barents Sea: Possible implications for palaeodrainage and subsidence, in Vorren, T.O., Bergsager, E., Dahl-Stamnes, Ø.A., Holter, E., Johansen, B., Lie, E., and Lund, T.B., eds., Arctic Geology and Petroleum Potential: Norwegian Petroleum Society (NPF) Special Publication 2, p. 481–493.

Bhattacharya, J.P., Copeland, P., Lawton, T.F., and Holbrook, J., 2016, Estimation of source area, river paleodischarge, paleoslope, and sediment budgets of linked deep-time depositional systems and implications for hydrocarbon potential: Earth-Science Reviews, v. 153, p. 77–110, doi:10.1016/j.earscirev.2015.10.013.

Bøe, R., Fossen, H., and Smelror, M., 2010, Mesozoic sediments and structures onshore Norway and in the coastal zone: Norway Geological Survey Bulletin, v. 450, p. 15–32.

Pózer Bue, E.P., and Andresen, A., 2014, Constraining depositional models in the Barents Sea region using detrital zircon U-Pb data from Mesozoic sediments in Svalbard, *in* Scott, R.A., Smyth, H.R., Morton, A.C., and Richardson, N., eds., Sediment Provenance Studies in Hydrocarbon Exploration and Production: Geological Society, London, Special Publication 386, p. 261–279, doi:10.1144/SP386.14.

Bugge, T., Elvebakk, G., Fanavoll, S., Mangerud, G., Smelror, M., Weiss, H.M., Gjelberg, J., Kristensen, S.E., and Nilsen, K., 2002, Shallow stratigraphic drilling applied in hydrocarbon exploration of the Nordkapp Basin, Barents Sea: Marine and Petroleum Geology, v. 19, no. 1, p. 13–37, doi:10.1016/S0264-8172(01)00051-4.

Bugge, T., Mangerud, G., Elvebakk, G., Mørk, A., Nilsson, I., Fanavoll, S., and Vigran, J.O., 1995, The Upper Palaeozoic succession on the Finnmark Platform, Barents Sea: Norsk Geologisk Tidsskrift, v. 75, p. 3–30.

Burgess, S.D., and Bowring, S.A., 2015, High-precision geochronology confirms voluminous magmatism before, during, and after Earth's most severe extinction: Science Advances, v. 1, no. 7, p. e1500470, doi:10.1126/sciadv.1500470.

Chen, Z.Q., and Benton, M.J., 2012, The timing and pattern of biotic recovery following the end-Permian mass extinction: Nature Geoscience, v. 5, no. 6, p. 375–383, doi:10.1038/ngeo1475.

Chumakov, N.M., and Zharkov, M.A., 2003, Climate during the Permian–Triassic biosphere reorganizations. Article 2. Climate of the Late Permian and Early Triassic: General inferences: Stratigraphy and Geological Correlation, v. 11, no. 4, p. 361–375.

Cocks, L.R.M., and Torsvik, T.H., 2006, European geography in a global context from the Vendian to the end of the Palaeozoic, *in* Gee, D.G., and Stephenson, R.A., eds., European Lithosphere Dynamics: Geological Society, London, Memoir 32, p. 83–95, doi:10.1144/GSL.MEM.2006.032.01.05.

Colpaert, A., Pickard, N., Mienert, J., Henriksen, L.B., Rafaelsen, B., and Andreassen, K., 2007, 3D seismic analysis of an Upper Palaeozoic carbonate succession of the eastern Finnmark Platform area, Norwegian Barents Sea: Sedimentary Geology, v. 197, no. 1-2, p. 79–98, doi:10.1016/j.sedgeo.2006.09.001.

Daradich, A., Mitrovica, J.X., Pysklywec, R.N., Willett, S.D., and Forte, A.M., 2003, Mantle flow, dynamic topography, and rift-flank uplift of Arabia: Geology, v. 31, no. 10, p. 901–904, doi:10.1130/G19661.1.

Ebert, K., 2009, Terminology of long-term geomorphology: A Scandinavian perspective: Progress in Physical Geography, v. 33, no. 2, p. 163–182, doi:10.1177/0309133309338138.

Ebert, K., Hall, A.M., Kleman, J., and Andersson, J., 2015, Unequal ice-sheet erosional impacts across low-relief shield terrain in northern Fennoscandia: Geomorphology, v. 233, p. 64–74, doi:10.1016/j.geomorph.2014.09.024.

Ehrenberg, S.N., Pickard, N.A., Svånå, T.A., Nilsson, I., and Davydov, V.I., 2000, Sequence stratigraphy of the inner Finnmark carbonate platform (Upper Carboniferous–Permian), Barents Sea correlation between well 7128/6–1 and the shallow IKU cores: Norsk Geologisk Tidsskrift, v. 80, no. 2, p. 129–161, doi:10.1080/002919600750042618.

Eide, C.H., Howell, J.A., and Buckley, S.J., 2014, Distribution of discontinuous mudstone beds within wave-dominated shallow-marine deposits: Star Point Sandstone and Blackhawk Formation, eastern Utah: American Association of Petroleum Geologists Bulletin, v. 98, no. 7, p. 1401–1429, doi:10.1306/01201413106.

Eide, C.H., Howell, J.A., and Buckley, S.J., 2015, Sedimentology and reservoir properties of tabular and erosive offshore transition deposits in wave-dominated, shallow-marine strata: Book Cliffs, USA: Petroleum Geoscience, v. 21, no. 1, p. 55–73, doi:10.1144/petgeo2014-015.

Faleide, J.I., Tsikalas, F., Breivik, A.J., Mjelde, R., Ritzmann, O., Engen, O., Wilson, J., and Eldholm, O., 2008, Structure and evolution of the continental margin off Norway and the Barents Sea: Episodes, v. 31, no. 1, p. 82–91.

Fjellanger, J., and Sørbel, L., 2007, Origin of the palaeic landforms and glacial impact on the Varanger Peninsula, northern Norway: Norsk Geologisk Tidsskrift, v. 87, p. 223–238.

Fjellanger, J., Sørbel, L., Linge, H., Brook, E.J., Raisbeck, G.M., and Yiou, F., 2006, Glacial survival of blockfields on the Varanger Peninsula, northern Norway: Geomorphology, v. 82, no. 3-4, p. 255–272, doi:10.1016/j.geomorph.2006.05.007.

Fossen, H., Mangerud, G., Hesthammer, J., Bugge, T., and Gabrielsen, R.H., 1997, The Bjorøy Formation: A newly discovered occurrence of Jurassic sediments in the Bergen arc system: Norsk Geologisk Tidsskrift, v. 77, no. 4, p. 269–287.

Gani, M.R., Bhattacharya, J.P., and MacEachern, J.A., 2005, Using ichnology to determine relative influence of waves, storms, tides, and rivers in deltaic deposits: Examples from Cretaceous Western Interior Seaway, USA, *in* MacEachern, J.A., Bann, K.L., Gingras, M.K., and Pemberton, S.G., eds., Applied Ichnology: Society for Sedimentary Geology (SEPM) Short Course Notes 52, p. 209–225.

Gawthorpe, R.L., and Leeder, M.R., 2000, Tectono-sedimentary evolution of active extensional basins: Basin Research, v. 12, no. 3-4, p. 195–218, doi:10.1046/j.1365-2117.2000.00121.x.

Geluk, M.C., 2005, Stratigraphy and Tectonics of Permo-Triassic Basins in the Netherlands and Surrounding Areas [Ph.D. thesis]: Utrecht, Netherlands, Utrecht University, 171 p.

Gjessing, J., 1978, 6. Vassdrag-og dalmønstre, *in* Norges Landformer: Oslo, Norway, Universitetsforlaget, 207 p.

Glørstad-Clark, E., Faleide, J.I., Lundschien, B.A., and Nystuen, J.P., 2010, Triassic seismic sequence stratigraphy and paleogeography of the western Barents Sea area: Marine and Petroleum Geology, v. 27, no. 7, p. 1448–1475, doi:10.1016/j.marpetgeo.2010.02.008.

Gradstein, F.M., Ogg, J.G., Schmitz, M.D., and Ogg, G.M., eds., 2012, The Geological Time Scale 2012: Amsterdam, Netherlands, Elsevier, 2 volumes, 1144 p.

Gudlaugsson, S.T., Faleide, J.I., Johansen, S.E., and Breivik, A.J., 1998, Late Palaeozoic structural development of the south-western Barents Sea: Marine and Petroleum Geology, v. 15, no. 1, p. 73–102, doi:10.1016/S0264-8172(97)00048-2.

Hadler-Jacobsen, F., Johannessen, E.P., Ashton, N., Henriksen, S., Johnson, S.D., and Kristensen, J.B., 2005, Submarine fan morphology and lithology distribution: A predictable function of sediment delivery, gross shelf-to-basin relief, slope gradient and basin topography: Geological Society, London, Petroleum Geology Conference Series, v. 6, p. 1121–1145.

Hall, A.M., 2015, Phanerozoic denudation across the Kola Peninsula, northwest Russia: Implications for long term stability of Precambrian shield margins: Norsk Geologisk Tidsskrift, v. 95, no. 1, p. 27–43.

Hall, A.M., Sarala, P., and Ebert, K., 2015, Late Cenozoic deep weathering patterns on the Fennoscandian shield in northern Finland: A window on ice sheet bed conditions at the onset of Northern Hemisphere glaciation: Geomorphology, v. 246, p. 472–488, doi:10.1016/j.geomorph.2015.06.037.

Helland-Hansen, W., Sømme, T.O., Martinsen, O.J., Lunt, I., and Thurmond, J., 2016, Deciphering Earth's natural hourglasses: Perspectives on source-to-sink analysis: Journal of Sedimentary Research, v. 86, no. 9, p. 1008–1033, doi:10.2110/jsr.2016.56.

Hendriks, B., Andriessen, P., Huigen, Y., Leighton, C., Redfield, T., Murrell, G., Gallagher, K., and Nielsen, S.B., 2007, A fission track data compilation for Fennoscandia: Norsk Geologisk Tidsskrift, v. 87, no. 1/2, p. 143–155.

Hendriks, B.W., and Andriessen, P.A., 2002, Pattern and timing of the post-Caledonian denudation of northern Scandinavia constrained by apatite fission-track thermochronology, *in* Doré, A.G., Cartwright, J.A., Stoker, M.S., Turner, J.P., and White, N., eds., Exhumation of the North Atlantic Margin: Timing, Mechanisms and Implications for Petroleum Exploration: Geological Society, London, Special Publication 196, p. 117–137, doi:10.1144/GSL.SP.2002.196.01.08.

Henriksen, E., Bjørnseth, H.M., Hals, T.K., Heide, T., Kiryukhina, T., Kløvjan, O.S., Larssen, G.B., Ryseth, A.E., Rønning, K., Sollid, K., and Stoupakova, A., 2011a, Uplift and erosion of the greater Barents Sea: Impact on prospectivity and petroleum systems, *in* Spencer, A.M., Embry, A.F., Gautier, D.L., Stoupakova, A.V., and Sørensen, K., eds., Arctic Petroleum Geology: Geological Society, London, Memoir 35, p. 271–281.

Henriksen, E., Ryseth, A.E., Larssen, G.B., Heide, T., Rønning, K., Sollid, K., and Stoupakova, A.V., 2011b, Tectonostratigraphy of the greater Barents Sea: Implications for petroleum systems *in* Spencer, A.M., Embry, A.F., Gautier, D.L., Stoupakova, A.V., and Sørensen, K., eds., Arctic Petroleum Geology: Geological Society, London, Memoir 35, p. 163–195.

Hochuli, P.A., and Vigran, J.O., 2010, Climate variations in the Boreal Triassic—Inferred from palynological records from the Barents Sea: Palaeogeography, Palaeoclimatology, Palaeoecology, v. 290, no. 1-4, p. 20–42, doi:10.1016/j.palaeo.2009.08.013.

Jakobsson, M., Mayer, L., Coakley, B., Dowdeswell, J.A., Forbes, S., Fridman, B., Hodnesdal, H., Noormets, R., Pedersen, R., Rebesco, M., and Schenke, H.W., 2012, The international bathymetric chart of the Arctic Ocean (IBCAO) version 3.0: Geophysical Research Letters, v. 39, no. 12, L12609, doi:10.1029/2012GL052219.

Kirchner, J.W., Finkel, R.C., Riebe, C.S., Granger, D.E., Clayton, J.L., King, J.G., and Megahan, W.F., 2001, Mountain erosion over 10 yr, 10 ky, and 10 my time scales: Geology, v. 29, no. 7, p. 591–594,

doi:10.1130/0091-7613(2001)029<0591:MEOYKY>2.0.CO;2.
Klausen, T.G., and Mørk, A., 2014, The Upper Triassic paralic deposits of the De Geerdalen Formation on Hopen: Outcrop analog to the subsurface Snadd Formation in the Barents Sea: American Association of Petroleum Geologists Bulletin, v. 98, no. 10, p. 1911–1941, doi:10.1306/02191413064.
Klausen, T.G., Ryseth, A.E., Helland-Hansen, W., Gawthorpe, R., and Laursen, I., 2014, Spatial and temporal changes in geometries of fluvial channel bodies from the Triassic Snadd Formation of offshore Norway: Journal of Sedimentary Research, v. 84, no. 7, p. 567–585, doi:10.2110/jsr.2014.47.
Klausen, T.G., Ryseth, A.E., Helland-Hansen, W., Gawthorpe, R., and Laursen, I., 2015, Regional development and sequence stratigraphy of the Middle to Late Triassic Snadd Formation, Norwegian Barents Sea: Marine and Petroleum Geology, v. 62, p. 102–122, doi:10.1016/j.marpetgeo.2015.02.004.
Klausen, T.G., Ryseth, A., Helland-Hansen, W., and Gjelberg, H.K., 2016, Progradational and backstepping shoreface deposits in the Ladinian to early Norian Snadd Formation of the Barents Sea: Sedimentology, v. 63, p. 893–916, doi:10.1111/sed.12242.
Kohn, B.P., Lorencak, M., Gleadow, A.J., Kohlmann, F., Raza, A., Osadetz, K.G., and Sorjonen-Ward, P., 2009, A reappraisal of low-temperature thermochronology of the eastern Fennoscandia Shield and radiation-enhanced apatite fission-track annealing, *in* Lisker, F., Ventura, B., and Glasmacher, U.A., eds., Thermochronological Methods: From Palaeotemperature Constraints to Landscape Evolution Models: Geological Society, London, Special Publication 324, p. 193–216, doi:10.1144/SP324.15.
Krumbein, W.C., and Garrels, R.M., 1952, Origin and classification of chemical sediments in terms of pH and oxidation-reduction potentials: The Journal of Geology, v. 60, no. 1, p. 1–33, doi:10.1086/625929.
Laberg, J.S., Andreassen, K., and Vorren, T.O., 2012, Late Cenozoic erosion of the high-latitude southwestern Barents Sea shelf revisited: Geological Society of America Bulletin, v. 124, no. 1-2, p. 77–88, doi:10.1130/B30340.1.
Larson, S.Å., Tullborg, E.L., Cederbom, C., and Stiberg, J.P., 1999, Sveconorwegian and Caledonian foreland basins in the Baltic Shield revealed by fission-track thermochronology: Terra Nova, v. 11, no. 5, p. 210–215, doi:10.1046/j.1365-3121.1999.00249.x.
Larson, S.Å., Cederbom, C.E., Tullborg, E.L., and Stiberg, J.P., 2006, Comment on "Apatite fission track and (U-Th)/He data from Fennoscandia: An example of underestimation of fission track annealing in apatite" by Hendriks and Redfield [Earth Planet. Sci. Lett. 236 (443–458)]: Earth and Planetary Science Letters, v. 248, no. 1-2, p. 561–568, doi:10.1016/j.epsl.2006.06.018.
Leturmy, P., Lucazeau, F., and Brigaud, F., 2003, Dynamic interactions between the Gulf of Guinea passive margin and the Congo River drainage basin: 1. Morphology and mass balance: Journal of Geophysical Research–Solid Earth, v. 108, no. B8, 2383, doi:10.1029/2002JB001927.
Li, Z., Bhattacharya, J., and Schieber, J., 2015, Evaluating along-strike variation using thin-bedded facies analysis, Upper Cretaceous Ferron Notom Delta, Utah: Sedimentology, v. 62, no. 7, p. 2060–2089.
Lidmar-Bergström, K., Ollier, C.D. and Sulebak, J.R., 2000, Landforms and uplift history of southern Norway: Global and Planetary Change, v. 24, no. 3, p. 211–231.
Lidmar-Bergström, K., Bonow, J.M., and Japsen, P., 2013, Stratigraphic landscape analysis and geomorphological paradigms: Scandinavia as an example of Phanerozoic uplift and subsidence: Global and Planetary Change, v. 100, p. 153–171, doi:10.1016/j.gloplacha.2012.10.015.
Mack, G.H., and James, W.C., 1994, Paleoclimate and the global distribution of paleosols: The Journal of Geology, v. 102, no. 3, p. 360–366, doi:10.1086/629677.
Mangerud, G., 1994, Palynostratigraphy of the Permian and lowermost Triassic succession, Finnmark Platform, Barents Sea: Review of Palaeobotany and Palynology, v. 82, no. 3-4, p. 317–349, doi:10.1016/0034-6667(94)90082-5.
Martinsen, O.J., Sømme, T.O., Thurmond, J.B., Helland-Hansen, W., and Lunt, I., 2010, Source-to-sink systems on passive margins: Theory and practice with an example from the Norwegian continental margin: Geological Society, London, Petroleum Geology Conference series, v. 7, p. 913–920.
McKie, T., and Williams, B., 2009, Triassic palaeogeography and fluvial dispersal across the northwest European Basins: Geological Journal, v. 44, no. 6, p. 711–741, doi:10.1002/gj.1201.
Miller, E.L., Soloviev, A.V., Prokopiev, A.V., Toro, J., Harris, D., Kuzmichev, A.B., and Gehrels, G.E., 2013, Triassic river systems and the paleo-Pacific margin of northwestern Pangea: Gondwana Research, v. 23, no. 4, p. 1631–1645, doi:10.1016/j.gr.2012.08.015.
Milliman, J.D., and Farnsworth, K.L., 2011, River Discharge to the Coastal Ocean: A Global Synthesis: Cambridge, UK, Cambridge University Press, p. 13–69, doi:10.1017/CBO9780511781247.003.
Mørk, A., and Elvebakk, G., 1999, Lithological description of subcropping Lower and Middle Triassic rocks from the Svalis Dome, Barents Sea: Polar Research, v. 18, no. 1, p. 83–104, doi:10.3402/polar.v18i1.6559.
Mørk, A., Elvebakk, G., Forsberg, A.W., Vigran, J.O., and Weitschat, W., 1999, The type section of the Vikinghøgda Formation: A new Lower Triassic unit in central and eastern Svalbard: Polar Research, v. 18, no. 1, p. 51–82.
Mørk, A., Knarud, R., and Worsley, D., 1982, Depositional and diagenetic environments of the Triassic and Lower Jurassic succession of Svalbard, *in* Embry, A.F., and Balkwill, H.R., eds., Arctic Geology and Geophysics: Canadian Society of Petroleum Geologists Memoir 8, p. 371–398.
Mørk, M.B.E., 1999, Compositional variations and provenance of Triassic sandstones from the Barents Shelf: Journal of Sedimentary Research, v. 69, no. 3, p. 690–710, doi:10.2110/jsr.69.690.
Müller, R., Nystuen, J.P., Eide, F., and Lie, H., 2005, Late Permian to Triassic basin infill history and palaeogeography of the Mid-Norwegian shelf–East Greenland region, *in* Wandas, B., Nystuen, J.P., Eide, E., and Gradstein, F.M., eds., Onshore-Offshore Relationships on the North Atlantic Margin: Norwegian Petroleum Society Special Publication 12, p. 165–189, doi:10.1016/S0928-8937(05)80048-7.
Nesje, A., and Whillans, I.M., 1994, Erosion of Sognefjord, Norway: Geomorphology, v. 9, no. 1, p. 33–45, doi:10.1016/0169-555X(94)90029-9.
Norina, D.A., Stupakova, A.V., and Kiryukhina, T.A., 2014, Depositional environments and the hydrocarbon generative potential of Triassic rocks of the Barents Sea Basin: Moscow University Geology Bulletin, v. 69, no. 1, p. 1–10, doi:10.3103/S0145875214010062.
Nystuen, J.P., 2008, Break-up of the Precambrian continent, *in* Ramberg, I.B., Bryhni, I., Nøttvedt, A., and Rangnes, K., eds., The Making of a Land—Geology: Trondheim, Norsk Geologisk Forening, p. 120–147.
Nystuen, J.P., Kjemperud, A.V., Müller, R., Adestål, V., and Schomacker, E.R., 2014, Late Triassic to Early Jurassic climatic change, northern North Sea region, *in* Martinius, A.W., Ravnås, R., Howell, J.A., Steel, R.J., and Wonham, J.P., eds., From Depositional Systems to Sedimentary Successions on the Norwegian Continental Margin: Chichester, UK, John Wiley & Sons, p. 59–99, doi:10.1002/9781118920435.ch3.
Ogg, J.G., Huang, C., and Hinnov, L., 2014, Triassic timescale status: A brief overview: Albertiana, v. 41, p. 3–30.
Olesen, O., Kierulf, H.P., Brönner, M., Dalsegg, E., Fredin, O., and Solbakk, T., 2013, Deep weathering, neotectonics and strandflat formation in Nordland, northern Norway: Norwegian Journal of Geology, v. 93, no. 3-4, p. 189–213.
Omma, J.E., 2009, Provenance of Late Paleozoic and Mesozoic Sediment to Key Arctic Basins: Implications for the Opening of the Arctic Ocean [Ph.D. dissertation]: Cambridge, UK, University of Cambridge, 222 p.
Péron, S., Bourquin, S., Fluteau, F., and Guillocheau, F., 2005, Paleoenvironment reconstructions and climate simulations of the Early Triassic: Impact of the water and sediment supply on the preservation of fluvial systems: Geodinamica Acta, v. 18, no. 6, p. 431–446, doi:10.3166/ga.18.431-446.
Puchkov, V.N., 2009, The evolution of the Uralian orogen, *in* Murphy, J.B., Keppie, J.D., and Hynes, A.J., eds., Ancient Orogens and Modern Analogues: Geological Society, London, Special Publication 327, p. 161–195, doi:10.1144/SP327.9.
Redfield, T.F., and Osmundsen, P.T., 2013, The long-term topographic response of a continent adjacent to a hyperextended margin: A case study from Scandinavia: Geological Society of America Bulletin, v. 125, no. 1-2, p. 184–200, doi:10.1130/B30691.1.
Reichow, M.K., Pringle, M.S., Al'Mukhamedov, A.I., Allen, M.B., Andreichev, V.L., Buslov, M.M., Davies, C.E., Fedoseev, G.S., Fitton, J.G., Inger, S., and Medvedev, A.Y., 2009, The timing and extent of the eruption of the Siberian Traps large igneous province: Implications for the end-Permian environmental crisis: Earth and Planetary Science Letters, v. 277, no. 1-2, p. 9–20, doi:10.1016/j.epsl.2008.09.030.
Retallack, G.J., 1997, Colour Guide to Paleosols: Chichester, UK, John Wiley & Sons Ltd., 175 p.
Riis, F., 1996, Quantification of Cenozoic vertical movements of Scandinavia by correlation of morphological surfaces with offshore data: Global and Planetary Change, v. 12, no. 1-4, p. 331–357, doi:10.1016/0921-8181(95)00027-5.
Roberts, D., and Lippard, S.J., 2005, Inferred Mesozoic faulting in Finnmark: Current status and offshore links: Geological Survey of Norway Bulletin, v. 443, p. 55–60.
Romans, B.W., Castelltort, S., Covault, J.A., Fildani, A., and Walsh, J.P., 2016, Environmental signal propagation in sedimentary systems across timescales: Earth-Science Reviews, v. 153, p. 7–29, doi:10.1016/j.earscirev.2015.07.012.
Ryseth, A., 2014, Sedimentation at the Jurassic-Triassic boundary, south-west Barents Sea, *in* Martinius, A.W., Ravnås, R., Howell, J.A., Steel, R.J., and Wonham, J.P., eds., From Depositional Systems to Sedimentary Successions on the Norwegian Continental Margin: Chichester, UK, John Wiley & Sons, p. 187–214.
Samuelsberg, T.J., Elvebakk, G. and Stemmerik, L., 2003, Late Palaeozoic evolution of the Finnmark Platform, southern Norwegian Barents Sea: Norwegian Journal of Geology/Norsk Geologisk Forening, v. 83, no. 4, p. 351–362.
Sellwood, B.W., and Valdes, P.J., 2006, Mesozoic climates: General circulation models and the rock record: Sedimentary Geology, v. 190, no. 1-4, p. 269–287, doi:10.1016/j.sedgeo.2006.05.013.
Sigmond, E.M.O., 1992, Bedrock Map of Norway and Adjacent Ocean Areas: Oslo, Norway, Geological Survey of Norway, scale 1:3,000,000.
Sømme, T.O., Helland-Hansen, W., Martinsen, O.J., and Thurmond, J.B., 2009a, Relationships between morphological and sedimentological parameters in source-to-sink systems: A basis for predicting semi-quantitative characteristics in subsurface systems: Basin Research, v. 21, no. 4, p. 361–387, doi:10.1111/j.1365-2117.2009.00397.x.
Sømme, T.O., Martinsen, O.J., and Thurmond, J.B., 2009b, Reconstructing morphological and depositional characteristics in subsurface sedimentary systems: An example from the Maastrichtian–Danian Ormen Lange system, More Basin, Norwegian Sea: American Association of Petroleum Geologists Bulletin, v. 93, no. 10, p. 1347–1377, doi:10.1306/06010909038.
Sømme, T.O., Martinsen, O.J., and Lunt, I., 2013, Linking offshore stratigraphy to onshore paleotopography: The Late Jurassic–Paleocene evolution of the south Norwegian margin: Geological Society of America Bulletin, v. 125, no. 7-8, p. 1164–1186, doi:10.1130/B30747.1.
Stoker, M.S., Stewart, M.A., Shannon, P.M., Bjerager, M., Nielsen, T., Blischke, A., Hjelstuen, B.O., Gaina, C., McDermott, K., and Ólavsdóttir, J., 2016, An overview of the Upper Palaeozoic–Mesozoic stratigraphy of the NE Atlantic region, *in* Péron-Pinvidic, G., Hopper, J.R., Stoker, M.S., Gaina, C., Doornenbal, J.C., Funck, T., and Árting, U.E., eds., The NE Atlantic Region: A Reappraisal of Crustal Structure, Tectonostratigraphy and Magmatic Evolution: Geological Society, London, Special Publication 447, https://doi.org/10.1144/SP447.2.
Sun, Y., Joachimski, M.M., Wignall, P.B., Yan, C., Chen, Y., Jiang, H., Wang, L., and Lai, X., 2012, Lethally hot

temperatures during the Early Triassic greenhouse: Science, v. 338, no. 6105, p. 366–370, doi:10.1126/science.1224126.

Svensen, H., Planke, S., Polozov, A.G., Schmidbauer, N., Corfu, F., Podladchikov, Y.Y., and Jamtveit, B., 2009, Siberian gas venting and the end-Permian environmental crisis: Earth and Planetary Science Letters, v. 277, no. 3-4, p. 490–500, doi:10.1016/j.epsl.2008.11.015.

Syvitski, J.P., and Milliman, J.D., 2007, Geology, geography, and humans battle for dominance over the delivery of fluvial sediment to the coastal ocean: The Journal of Geology, v. 115, no. 1, p. 1–19, doi:10.1086/509246.

Talwani, M., and Eldholm, O., 1977, Evolution of the Norwegian-Greenland Sea: Geological Society of America Bulletin, v. 88, no. 7, p. 969–999, doi:10.1130/0016-7606(1977)88<969:EOTNS>2.0.CO;2.

Taylor, A.M., and Goldring, R., 1993, Description and analysis of bioturbation and ichnofabric: Journal of the Geological Society [London], v. 150, no. 1, p. 141–148, doi:10.1144/gsjgs.150.1.0141.

ten Brink, U., and Stern, T., 1992, Rift flank uplifts and hinterland basins: Comparison of the Transantarctic Mountains with the Great Escarpment of southern Africa: Journal of Geophysical Research–Solid Earth, v. 97, no. B1, p. 569–585, doi:10.1029/91JB02231.

Vigran, J.O., Mangerud, G., Mørk, A., Worsley, D., and Hochuli, P.A., 2014, Palynology and Geology of the Triassic Succession of Svalbard and the Barents Sea: Geological Survey of Norway Special Publication 14, 274 p.

von Blanckenburg, F., 2005, The control mechanisms of erosion and weathering at basin scale from cosmogenic nuclides in river sediment: Earth and Planetary Science Letters, v. 237, p. 462–479, doi:10.1016/j.epsl.2005.06.030.

Walker, R.G., 1965, June. The origin and significance of the internal sedimentary structures of turbidites, *in* Proceedings of the Yorkshire Geological and Polytechnic Society: Geological Society of London, v. 35, no. 1, p. 1–32.

Wellner, R., Beaubouef, R., VanWagoner, J.C., Roberts, H.H., and Sun, T., 2005, Jet-plume depositional bodies—The primary building blocks of Wax Lake delta: Transactions of the Gulf Coast Association of Geological Societies, v. 55, p. 867–909.

Wernicke, B., 1985, Uniform-sense normal simple shear of the continental lithosphere: Canadian Journal of Earth Sciences, v. 22, no. 1, p. 108–125, doi:10.1139/e85-009.

Wignall, P.B., Morante, R., and Newton, R., 1998, The Permo-Triassic transition in Spitsbergen: $\delta^{13}C_{org}$ chemostratigraphy, Fe and S geochemistry, facies, fauna and trace fossils: Geological Magazine, v. 135, no. 1, p. 47–62, doi:10.1017/S0016756897008121.

Winsborrow, M.C., Andreassen, K., Corner, G.D., and Laberg, J.S., 2010, Deglaciation of a marine-based ice sheet: Late Weichselian palaeo-ice dynamics and retreat in the southern Barents Sea reconstructed from onshore and offshore glacial geomorphology: Quaternary Science Reviews, v. 29, no. 3-4, p. 424–442, doi:10.1016/j.quascirev.2009.10.001.

Worsley, D., 2008, The post-Caledonian development of Svalbard and the western Barents Sea: Polar Research, v. 27, no. 3, p. 298–317, doi:10.1111/j.1751-8369.2008.00085.x.

Ziegler, P.A., 1992, North Sea rift system: Tectonophysics, v. 208, no. 1-3, p. 55–75, doi:10.1016/0040-1951(92)90336-5.

Science Editor: Aaron J. Cavosie
Associate Editor: Henning Dypvik

Manuscript Received 24 August 2016
Revised Manuscript Received 26 April 2017
Manuscript Accepted 14 June 2017

Printed in the USA